THE ASTROPHYSICAL JOURNAL, 424:84–105, 1994 March 20

FUELING NUCLEAR ACTIVITY IN DISK GALAXIES: STARBURSTS AND MONSTERS

CLAYTON H. HELLER AND ISAAC SHLOSMAN
Department of Physics and Astronomy, University of Kentucky, Lexington, KY 40506-0055
Received 1993 February 8; accepted 1993 September 28

ABSTRACT

We study the evolution of the gas distribution in a globally unstable galactic disk with a particular emphasis on the gasdynamics in the central kiloparsec and the fueling activity there. The two-component self-gravitating disk is embedded in a responsive halo of comparable mass. The gas and stars are evolved using a three-dimensional hybrid smoothed particle hydrodynamics/N-body code and the gravitational interactions are calculated using a hierarchical TREE algorithm. A massive "star formation" is introduced when the gas becomes Jeans unstable and locally exceeds the critical density of $\sim 100\ M_\odot\ \mathrm{pc}^{-3}$. The newly formed OB stars deposit energy in the gas by means of radiation-driven winds and supernovae. This energy is partially thermalized (efficiency of a few percent); the rest is radiated away. Models without star formation are evolved for a comparison. The effect of a massive object at the disk center is studied by placing a "seed" black hole (BH) of $5 \times 10^7\ M_\odot$ with an accretion radius of 20 pc. The tendency of the system to form a massive object "spontaneously" is tested in models without the BH.

We find that for models *without* star formation the bar- or dynamical friction-driven inflows lead to 1) domination of the central kpc by a few massive clouds that evolve into a single object probably via a cloud binary system, with and without a "seed" BH, 2) accretion onto the BH which has a sporadic character, and 3) formation of remnant disks around the BH with a radius of 60–80 pc which result from the capture and digestion of clouds. For models *with* star formation, we find that 1) the energy input into the gas induces angular momentum loss and inflow rates by a factor <3, 2) the star formation is concentrated mainly at the apocenters of the gaseous circulation in the stellar bar and in the nuclear region, 3) the nuclear starburst phase appears to be very luminous $\sim 10^{45}$–10^{46} erg s^{-1} and episodic with a typical single burst duration of $\sim 10^7$ yr, and 4) the starburst phase coincides with both the gas becoming dynamically important and the catastrophic growth of the BH. It ends with the formation of cold residual <1 kpc radius gas disks. Models without the "seed" BH form <1 kpc radius *fat* disks which dominate the dynamics. *Gaseous* bars follow, drive further inflow, and may fission into a massive cloud binary system at the center.

Subject headings: galaxies: evolution — galaxies: kinematics and dynamics — galaxies: Seyfert — galaxies: starburst — galaxies: structure — hydrodynamics — quasars: general — stars: formation

1. INTRODUCTION

The central regions of some disk galaxies are sites of pronounced activity. It is generally accepted that this activity results from accretion onto a supermassive black hole (BH) in active galactic nuclei (AGNs) and a high formation rate of massive stars in nuclear starburst galaxies (e.g., reviews by Begelman, Blandford, & Rees 1984; Telesco 1988). The limited efficiency of both processes requires a large amount of material to be processed in order to achieve the observed level of energy output. This may involve as much as $\sim 10^{10}\ M_\odot$, which is a few percent of the total galactic mass, and probably a large fraction of the interstellar medium (ISM) in the parent galaxies of the most luminous objects. The majority of AGNs and starbursts probably consume less material. However, even this amount seems to be dynamically important when compared with the total mass residing within the inner kiloparsec.

While the ISM necessary to fuel this activity can be found in the main body of the host galaxy, it is separated by an angular momentum barrier from the central regions. An efficient mechanism for extraction of angular momentum from the gas on a dynamical timescale is required in order to obtain the necessary high inflow rates toward the inner disk where activity is observed: $\sim 10^{-4}$–10^{-3} pc in the case of an AGN and $\sim$1–2 kpc for a nuclear starburst. Possible mechanisms have been reviewed by Shlosman, Begelman, & Frank (1990), who argued in favor of global nonaxisymmetric instabilities both in the stellar disk, subject to intrinsic and extrinsic triggers, *and* in the growing central gas accumulation. Stellar bars channeling the gas toward the inner galaxy in order to fuel the activity there were originally suggested by Simkin, Su, & Schwarz (1980), and much of the numerical activity since has been directed to study the gaseous flows in a barred *stellar* potential. However, there are indications that the *gas* plays an important if not dominant role in the dynamics of the central few hundred parsecs. If this is the case, the onset and development of runaway gravitational instabilities on scales $\lesssim 500$ pc should differ dramatically from those in the large-scale stellar disk. Because of the dissipational and collisional nature of the gas, it tends to reduce dispersion velocities and undergo fragmentation. A simple extrapolation of stellar dynamical processes to gas is therefore not justified.

There are some additional aspects to this problem. First, because the formation of the inner parts of galaxies should involve a good deal of dissipation, it is tempting to relate the origin of the supermassive BH itself to the inflow, perhaps at an early epoch of disk formation. Second, if this inflow is accompanied by a starburst in the inner few kpc where the gas is the most compressed, the gas clouds can acquire large velocity dispersions perpendicular to the disk plane and contribute to the formation of a bulge.

A rapidly mounting body of observational evidence, which is briefly reviewed in the next section, speaks in favor of radial redistribution of the ISM and its accumulation in the nuclear regions, where it becomes a significant fraction of the dynamical mass. The kinematics of molecular gas in active galaxies reflect both the action of gravitational torques and interaction with energetic stellar winds and supernovae ejecta whose energy is primarily injected into the central ~ 1 kpc region.

Considerable effort to model numerically the gaseous response to the nonaxisymmetric background potential on the galactic scale was made during the last couple of decades (e.g. Sorensen, Matsuda, & Fujimoto 1976; Huntley 1978; Huntley, Sanders, & Roberts 1978; Sanders & Tubbs 1980; van Albada & Roberts 1981; Schwarz 1984; Combes & Gerin 1985; Fukunaga & Tosa 1991; Athanassoula 1992a, b; Wada & Habe 1992, and others; see also reviews by Toomre 1981; Athanassoula 1984; Sellwood 1992; Sellwood & Wilkinson 1993). This has provided an important insight into the formation and maintenance of spiral structure in disk galaxies. In some of the works, it was claimed that a nonaxisymmetric potential had created a radial gas inflow, but a lack of resolution has limited their ability to follow these flows for more than a decade in radius. All of these studies have been two-dimensional, and most have neglected two major factors: self-gravity and the high degree of clumpiness in the gas, although these can be viewed as salient properties of the ISM. They have also avoided a dynamically self-consistent treatment by *imposing* an oval or spiral distortion of the underlying gravitational potential and ignoring the back-reaction of the gaseous component, thus using the gas merely as a tracer of the stellar gravitational field. Alternatively, some theoretical works have emphasized the dynamical importance of gas in the local (e.g., Julian & Toomre 1996; Lubow, Balbus, & Cowie 1986; Balbus 1988; Lubow 1988; Bertin et al. 1989) and global (Norman 1988; Shlosman, Frank, & Begelman 1988, 1989) phenomena in the disks of spiral galaxies.

Shlosman & Noguchi (1993) have performed a parameter study and found that the gaseous response to a global instability in the stellar disk differs with gas mass fraction: when it is less than $\sim 10\%$, the gas is channeled inward by a growing stellar bar. For higher gas fractions, the gas becomes highly inhomogeneous and the bar instability is heavily damped. The gas then falls toward the inner kiloparsec due to a dynamical friction. In the present work we extend the previous analysis by Shlosman and Noguchi of the global stability of self-gravitating two-component galactic disks to include the effects of massive star formation and concentrate on studying the gas dynamics in the inner disks, down to ~ 50 pc from the center. We aim at understanding the physical processes which lead to nuclear starbursts and to the rapid growth of the central BH. Owing to the many uncertainties involving star formation and the related energy deposition in the ISM, as well as limitations following from our numerical approach, this analysis should be viewed as a qualitative one. The models without star formation have been run for comparison, and they represent the extreme case when the dissipation in the gas is not compensated by local heating above 10^4 K, thus emphasizing the clumpiness in the ISM.

Non axisymmetric instabilities in the galactic disks which result in ~ 10 kpc–scale gaseous inflows can also be triggered by extrinsic factors, such a tidal interactions between galaxies and galactic mergers (Noguchi 1988; Hernquist 1989). Results presented in this paper should also be applicable, in principle, to the case of extrinsic triggers, if the barlike mode is dominant on the larger scale. We do not expect that the gasdynamical processes within the inner kiloparsec would be strongly modified by the differences between "spontaneous" and tidally induced stellar bars. However, this deserves a separate study.

Section 2 is devoted to the observational evidence of large-scale redistribution of molecular gas in disk galaxies. We explain the numerical method in § 3 and present results of numerical simulations with and without star formation in § 4. We also discuss the specifics of the central kiloparsec, the growth of the central BH and the global stability of nuclear gaseous disks. Additional comments and conclusions are presented in the last section.

2. CENTRAL KILOPARSEC: DYNAMIC STATUS OF MOLECULAR GAS

Our understanding of the molecular gas distribution and kinematics in external galaxies suffers from low angular resolution typically corresponding to a linear resolution $\gtrsim 1$ kpc and, in a few exceptional cases, to $\gtrsim 100$ pc. It is based on observations of the CO molecule which is a tracer of a low-density $\lesssim 10^3$ cm^{-3} gas and on a number of other molecular species, such as CN, C_2H, and HC_3N, all of which can be found in denser regions and are therefore more appropriate to use when studying the inner kiloparsec.

Perhaps the most intriguing aspect of the high-resolution observations is the prevalence of morphologically disturbed molecular gas in the inner regions. The molecular gas within a kiloparsec of galactic centers is found either in elongated structures described as molecular bars or in nuclear rings. The former morphology shows clear noncircular motions, while the latter one serves to measure the total mass within the ring. In addition, the nuclear gas seems to be highly nonuniform. Gaseous barlike structures have been observed on scales down to 100–300 pc (semimajor axis) and are typically a few times smaller than the large-scale stellar bars. They also may contain solid-body rotating disks or rings in the innermost regions. Recent reviews of nuclear molecular gas (Henkel, Baan, & Mauersberger 1991; Sofue 1991; Young & Scoville 1991; Scoville et al. 1993, and references therein) have discussed these aspects of the molecular gas distribution and emphasized the compactness of nuclear gas concentrations. The latter increases with far-infrared luminosity and is most prominent in ultraluminous infrared galaxies. Highly compact molecular gas concentrations have also been observed recently in the early-type disks—S0's, Sa's and Sab's (Meixner et al. 1990; Braine & Combes 1992; Wrobel & Kenney 1992), which is particularly interesting because this is a preferred site for Seyfert nuclei.

The kinematics of molecular gas in the innermost disks indicate radial velocities of ~ 100 km s^{-1} and rotation with the same typical velocities. The rotation provides a measure of the central dynamical mass of a few 10^8–10^9 $M_\odot$. Gas–to–dynamical mass ratios within the molecular gas concentration lie between 0.1–0.6 (e.g., Sofue 1991; Kenney et al. 1992; Scoville et al. 1993; Turner 1993; etc.), although the intensity-to-mass conversion factor for the CO is not without controversy.

Nuclear molecular "bars" have been mapped in galaxies with prominent stellar bars as well as in apparently unbarred systems. A clear correlation exists between central activity and stellar bars, based on optical, Hα, radio, and infrared surveys (e.g., Adams 1977; Simkin, Su, & Schwarz 1980; Hummel 1981; Balzano 1983; Hawarden et al. 1986; Devereux 1987;

Jackson et al. 1987; Dressel 1988; Puxley, Hawarden, & Mountain 1988, and many others; however, see Braine & Combes 1992). The detection of a bar itself is often confusing. Even strong stellar bars may not be recognized unless imaged in the near-infrared (e.g., Hackwell & Schweizer 1983; Scoville et al. 1988; Thronson et al. 1989). Classification of barred and unbarred systems in the RSA (Sandage & Tammann 1981) and the RC2 Catalogues (de Vaucouleurs, de Vaucouleurs, & Corwin 1976) are in frequent disagreement, especially for the later type Sc systems (Condon 1983). In addition, oval distortions of stellar disks are probably universal and produce the same effects on the gas as bars do (e.g., Kormendy 1982).

Large concentrations of molecular gas are accompanied by extensive star formation and/or accretion onto the massive BH in the central regions of active galaxies. Indications of this come from different wavelengths: from infrared through optical (H II regions) to radio (synchrotron emission). Nuclear starbursts may require that the initial mass function be skewed toward more massive stars (e.g., Rieke et al. 1980; Kennicutt et al. 1987; Wright et al. 1988; Scalo 1989; Rieke et al. 1993). Much of the information on these objects comes from the *Infrared Astronomical Satellite* (*IRAS*), in the range of 12–100 μm. The warm emission component in the far-infrared band originates from dust-reprocessed ultraviolet stellar light and is an acceptable measure of the stellar bolometric luminosity. Massive stars coexisting with the molecular clouds are capable of heating dust grains to temperatures well above 100 K. A large number of massive stars is required in order to be consistent with the estimated amount of warm dust, thereby imposing a lower limit on the star formation rate.

We conclude that the available data on the distribution and kinematics of molecular gas in disk galaxies supports the idea of the ongoing rearrangement of this gas on the galactic scale. This as well as a correlation between the level of nuclear activity and the degree of central concentration of dynamically perturbed gas has provided a strong incentive for our theoretical modeling of gasdynamical processes in disk galaxies.

3. NUMERICAL METHOD

We have used a TREE algorithm (Barnes & Hut 1986; Hernquist 1987) to calculate the gravitational interactions between stars and gas in globally unstable disk galaxies consisting of three components: stars, gas, and a live halo. The gas is evolved by using a smooth particle hydrodynamics (SPH) method, which is a fully Lagrangian scheme where the continuous physical fields, density, and velocity are approximated by a finite set of points which are often referred to as particles (Lucy 1977; Monaghan 1982). The advantages and shortcomings in using SPH have been recently summarized by Monaghan (1992). The SPH algorithm we have adopted is an advanced version of the one used by Heller (1991). Our modifications include dynamic gravitational softening lengths for the gas, multiple timesteps, and vectorization and parallelization of large sections of the code which involve the TREE building and descents.

3.1. *Hydrodynamics*

The equations of motion for the gas particles are based on smoothed field values computed by performing averages over local volumes as defined by a kernal interpolation formula,

$$\langle A(\boldsymbol{r})\rangle \simeq \sum_i \frac{A_i}{n_i} W(\boldsymbol{r}, \boldsymbol{r}_i, h) , \quad (1)$$

where $A_i \equiv A(\boldsymbol{r}_i)$ is the field, $\boldsymbol{r}_i$ is the position vector of a particle, n_i is the local number density of particles, W is the interpolating kernel, and h is the smoothing length which defines the spatial resolution.

For the spherically symmetric spline kernel that we use, only particles within a radius of $2h$ will contribute to the sums. The smoothing length of an individual particle is determined by the radius of a sphere centered on the particle which contains a fixed number of neighbors. The spatial resolution is therefore dynamic, and the smoothed quantities are computed with approximately the same accuracy everywhere.

The introduction of an artificial viscosity is necessary for the accurate treatment of shocks (Monaghan & Gingold 1983). We use the form given by equation (2.25) in Hernquist & Katz (1989) with $\alpha = 0.5$ and $\beta = 1.0$.

3.2. *Gravity*

The gravitational forces between gas, stars, and halo particles are computed by a hierarchical TREE method which allows the gravitational potential of N mass points to be calculated in $N \log N$ time. To obtain the gravitational force acting on a particle, the mass points are subdivided into groups, whose spatial size increases with increasing distance from the particle. The logarithmic scaling results from approximating the mass distribution within each group by a multiple expansion and then summing the particle-group interactions. The error introduced in each interaction is controlled so that the nearest groups will degenerate to the limiting case of a single mass point. In this way the local contribution to the acceleration is generally computed as a direct sum over nearby particles. The tolerance criteria used is $s/d < \theta$, where s is the size of the cell, d is the distance between the cell and the point where the potential is being computed, and θ is a fixed tolerance parameter. It should be noted that the multipole expansion of the cell potential is essentially a power series in s/d (Hernquist 1987). For the computations presented here we take $\theta = 0.8$ and include terms up to quadrupole in the cell expansions.

The Keplerian potential between two particles is replaced by the softened form given by Hernquist & Katz (1989), in order to prevent numerical divergencies and to reduce the two-body relaxation. It is based on the assumption that the local mass distribution surrounding the particles is distributed according to the SPH kernel function. The potential is then computed between a point and this spherically symmetric mass distribution, parameterized by the softening length, ϵ, where the exact Keplerian form is obtained for $r \geq 2\epsilon$. For the collisionless particles the softening length is held constant, $\epsilon_* = 200$ pc, which is the average interparticle distance at 1 kpc. For the gas, the softening length is set equal to the smoothing length, $\epsilon_g = h$. For the cells the mass-weighted average is used. An SPH neighborhood of 38 gas particles results in a gas softening length which is approximately equal to the local mean particle separation. To avoid excessive computing time, we impose a lower limit, $\epsilon_{\min} = 75$ pc, on the gravitational softening parameter ϵ_g, for models without star formation.

3.3. *Time Steps*

The dynamic range which is relevant for our galaxy models involves some three to four orders of magnitude in radius and density. Such a large range requires that multiple time step sizes be employed, a procedure accomplished with a hierarchy of time bins. The top bin is assigned a step size which rep-

resents the maximum system step size allowed, then each subsequent bin has a step size which is one-half the value of the bin above it. Particles are placed in the bins according to their individually computed step sizes, which for the gas particles include the Courant condition and the condition demanded by the diffusive terms:

$$\delta\tau_i = C \min\left(\sqrt{\frac{h_i}{F_i}}\,;\,\frac{h_i}{\sigma_i}\right) \tag{2}$$

(Monaghan 1988), where $C \sim 0.3$ is the Courant number, F_i is the acceleration experienced by particle i, and the viscosity parameter σ_i is defined in Hernquist & Katz (1989). The time step size for a collisionless particle is given by

$$\delta\tau_i = \eta \frac{m_i|\mathscr{E}_i|}{\Delta T_i} = \eta \frac{|\mathscr{E}_i|}{\|\dot{\boldsymbol{r}}_i\|\,\|\ddot{\boldsymbol{r}}_i\|}\,, \tag{3}$$

where η is a tolerance parameter, m_i is the mass of a collisionless particle, and $\mathscr{E}_i$ and T_i are, respectively, the total energy per unit mass and kinetic energy of particle i. At times ΔT_i can be very small, so in practice we use

$$\frac{1}{\delta\tau_i} = \min\left(\frac{\|\dot{\boldsymbol{r}}_i\|\,\|\ddot{\boldsymbol{r}}_i\|}{\eta|\mathscr{E}_i|}\,;\,\frac{1}{\delta\tau_{\min}}\right), \tag{4a}$$

where $\delta\tau_{\min}$ is the minimal allowable time step for collisionless particles. The particles in each bin are advanced together. The order in which the bins are selected is discussed by Whitehurst (1988).

3.4. *Testing the Algorithm: Shocks and Polytropes*

A simulation of a collision between two nongravitating isothermal sheets of gas was performed in order to test the algorithm's ability to properly address isothermal shocks and to avoid numerical diffusion. The particles were initially located on a grid with a spacing of $dx = dy = 0.03$ units and with equal masses of value $m = p\,dx\,dy = 1\,dx\,dy$. Particles located at $x < 0$ had initial velocities of $v_0 = 1$ (Mach 1) while those with $x > 0$ had $v_0 = -1$.

Shown in Figure 1*a* is the Mach 2 shock density profile at $\tau = 0.5$. The algorithm adequately reproduced the analytic profile given by the solid curve. These profiles were obtained from the central region of the sheet where the gas was unperturbed by the inward propagating rarefaction wave.

In the second test we simulate a self-gravitating polytropic gas sphere in hydrostatic equilibrium and undergoing radial pulsations. The SPH particles ($N = 4096$) were initially given the radial density distribution of a $n = 1.5$ polytrope. This distribution was relaxed to a hydrostatic configuration by evolv-

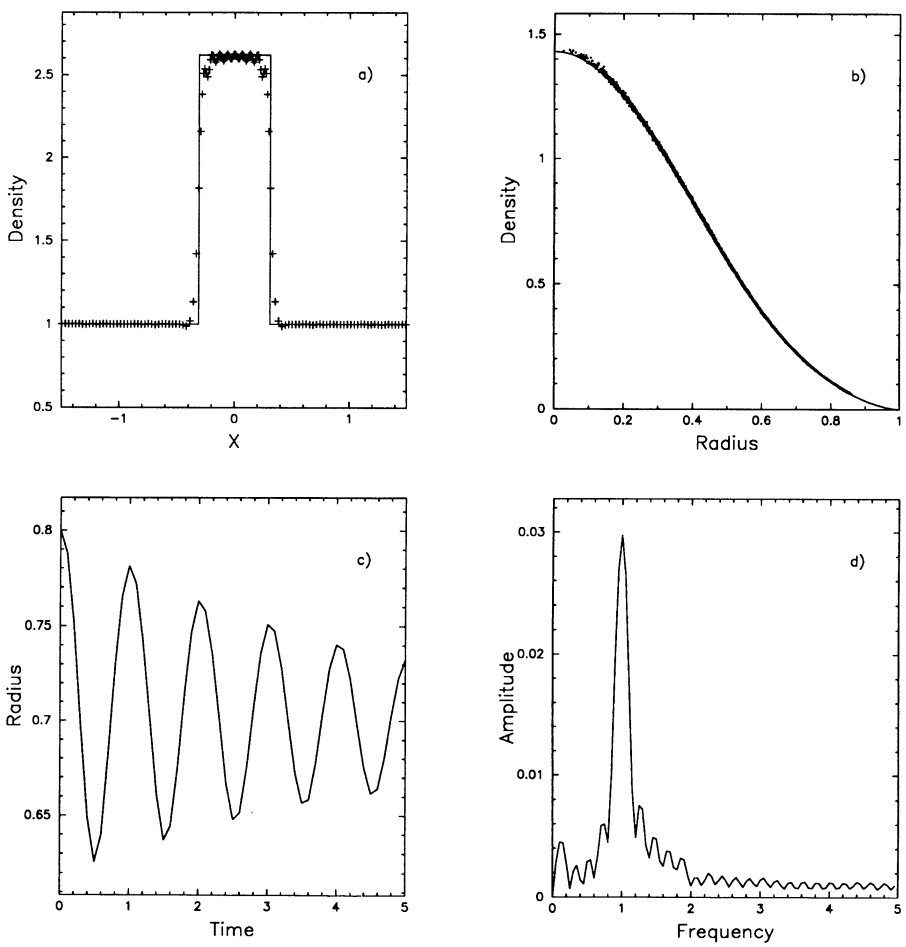

FIG. 1.—(*a*) Shock profile of colliding isothermal sheets of gas. The analytic solution is given by the solid curve. (*b*) Radial mass distribution of a polytropic gas sphere. The analytic solution is given by the solid curve. (*c*) Radial pulsations of a polytropic mass sphere, depicted by plotting the radius of the mass shell, $M_r = 0.8$, vs. time in units of the LAWE fundamental radial period. (*d*) Power spectrum of (*c*), showing that the numerical simulation successfully produced the expected pulsation frequency.

ing it with a frictional term added to the equation of motion (Lucy 1977; Heller 1991). The radial density distribution of the relaxed system is compared with the analytical solution in Figure 1*b*. Without the dynamic softening, large deviations would have occurred near the center.

The relaxed polytrope was then homologeously expanded by 15% in radius and evolved without the frictional term. The resulting radial pulsations are shown in Figure 1*c* where the radius of the mass shell, $M_r = 0.8$ has been plotted versus time in units of the fundamental radial pulsation period as determined from the linear adiabatic wave equation (Cox 1980). The amplitude of the pulsation decays with time due to the presence of the artificial viscosity. A power spectrum is given in Figure 1*d* and shows that the numerical simulation successfully produced the expected pulsation frequency. The Nyquist frequency and frequency resolution are 5.0 and 0.05 cycles per unit time, respectively, with the frequency at which the power is maximal, being equal to unity within the frequency resolution.

3.5. *Initial Conditions*

For the initial (gas and stellar) density distribution we have selected the Fall & Efstathiou (1980) disk-halo model which consists of an exponential disk and a spherical halo. This model is less concentrated than Kuzmin-Toomre models (Toomre 1962) and has a flat rotation curve in the outer disk. The halo-to-disk mass ratio is taken as unity, which ensures that the pure stellar model for the disk will be globally unstable and form a large-scale bar. The units of mass, distance, and time are $M_{\rm gal} = 10^{11}\ M_\odot$, $R_{\rm gal} = 10$ kpc and the dynamical time $\tau_{\rm dyn} \equiv (R_{\rm gal}^3/GM_{\rm gal})^{1/2} = 4.7 \times 10^7$ yr. The stellar disk rotation period in these units corresponds to $2\pi\tau_{\rm dyn}$ at 10 kpc. The radial and vertical scale heights in the stellar disk have been chosen as 2.85 kpc and 0.5 kpc, respectively, and the rotational velocity turnover radius at $r_m = 7$ kpc. The vertical scale height in the gas is 0.25 kpc. An isothermal equation of state is used for the gas with a temperature of 10^4 K, except for regions of star formation (see § 3.6). This temperature represents a random motion of molecular clouds in the disk. The halo contains 10,240 collisionless particles, and the disk contains 16,384 collisionless and 8,192 collisional SPH particles.

This distribution is not in exact virial equilibrium and must be allowed to relax. This is accomplished following the procedure used by Shlosman & Noguchi (1993), where the halo particles are given an (isotropic) velocity dispersion which satisfies the virial equation for a nonrotating sphere, while freezing the disk particles and evolving the model for some 15 dynamical times. The disk particles are then "warmed up" by giving them Keplerian velocities defined by the local gravitational potential. In addition, the stellar disk particles are given velocity dispersions based on Toomre's stability criterion (Toomre 1964) with $Q_* = 1.5$. We also correct for asymmetric drift (e.g., Binney & Tremaine 1987). The modified rotation curve rises linearly from the center to about 3–4 kpc then flattens at approximately 5–6 kpc with $r_m \sim 6$ kpc (Fig. 2).

3.6. *The BH Accretion and Star Formation*

Massive stars recycle the ISM. On the galactic scale, they show a tight correlation with the distribution of giant molecular clouds—a sign of generic relationship. Massive stars also provide the major energy source for the ISM by means of line-driven winds and supernovae explosions. We attribute this energy deposition to the star formation itself, for brevity. Both the winds and supernovae deposit about equal amounts of

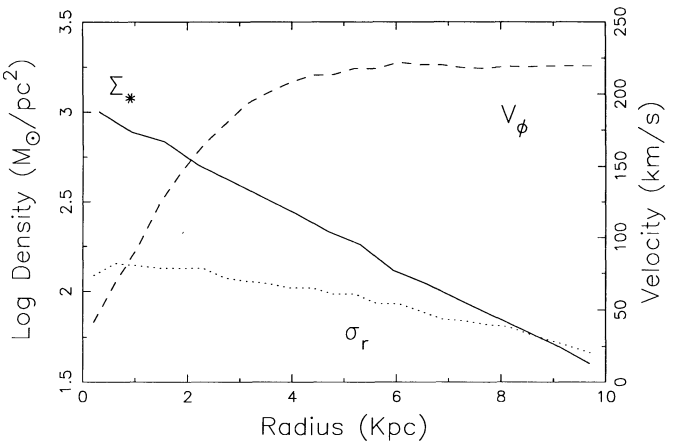

FIG. 2.—Initial conditions for a generic model (A0). Profiles of stellar surface density (*solid line*), rotation velocity (*dashed line*), and radial dispersion velocity (*dotted line*) in the disk.

energy though on different timescales (e.g., Salpeter 1976). Only a few percent of this energy is typically retained by the ISM; the rest is radiated away before thermalizing.

The physics of star formation is sufficiently unknown at the moment to justify a phenomenological approach. When the density in the locally gravitationally *unstable* gas exceeds some critical value, typically 100 $M_\odot$ pc^{-3} (which corresponds to the gas particle smoothing length becoming smaller than a specified value $h_{\rm OB}$), the gas particle undergoes "star formation." Observational support for this approach is given, for example, by Kennicutt (1989). This event results in the deposition of energy into the gas and an increase in the gas pressure which is maintained over a period of time. The increase of the pressure over the isothermal value during a single time step of duration $\Delta\tau_i$ is given by

$$\tilde{p}_i = p_i + \Delta p_i \frac{\Delta\tau_i}{\tau_{\rm OB}}, \tag{4b}$$

with

$$\Delta p_i = \xi \frac{b_i E_{\rm OB}}{h_i^3} \quad \text{for } h_i \le h_{\rm OB}, \tag{5}$$

where $E_{\rm OB} = 3 \times 10^{51}$ ergs is the total kinetic energy deposited by radiation-driven winds from an OB star with a mass $m_{\rm OB} = 15\ M_\odot$ during its main sequence lifetime of $\tau_{\rm OB} = 10^6$ yr, b_i is the ratio of SPH particle mass to $m_{\rm OB}$, and $\xi = 0.05$ is the conversion efficiency of wind kinetic energy into gas motion (e.g., Chevalier 1974; Salpeter 1976; Spitzer 1978). After the time period $\tau_{\rm OB}$ has elapsed, the pressure is incremented by an additional Δp_i to simulate the effect of a supernova which deposits the same $E_{\rm OB}$ during $\tau_{\rm SN} = 10^4$ yr. We ignore effects related to the initial mass function (IMF), assuming that only massive stars are forming, leaving no remnants at the end of their evolutionary path. Although evidence exists that the IMF in starburst galaxies is modified toward more massive stars (§ 2), our assumption may overestimate the rate of energy deposition. We therefore compensate for this effect by conservatively limiting the efficiency ξ to a few percent.

Massive star formation in our models is concentrated with the central 5–6 kpc, where the surface density of the gas is high enough to drive it quickly to Jeans instability. Because the lifetime of an OB star is generally less than the characteristic

rise time for this instability, they are expected to substantially influence the collapse on gravitationally unstable ~ 10–100 pc scales. The immediate result, as expected, is to prevent large fragments from forming and to limit the lifetime of smaller fragments. Therefore, models with star formation do *not* require the imposition of a minimal gravitational softening length in the gas. Typically, a fraction ($\propto \xi^{-1}$) of the contracting clump mass becomes "active," which is sufficient to reverse the local collapse and in many cases disperse the clump completely. This is a self-regulating process, and the fraction of the gas converted into massive stars is not prescribed *ab initio* but depends on the conversion efficiency of wind and supernovae expansion energy into gas motion.

To simulate the effect of a massive BH at the center of a galaxy, we fix a single SPH particle at the center of mass of the disk. The particle starts with a "seed" mass of $M_{\rm BH} = 5 \times 10^7$ $M_\odot$ and accretes any *gas* particles within a volume of radius $r_{\rm acc} = 20$ pc. Realistically, we expect magnetic torques to take over somewhere within this radius (Emmering, Blandford, & Shlosman 1992), and the adopted inner boundary conditions are for simplicity only. This should have only a minor effect on the growth rate of the BH. The momentum of an absorbed particle is considered lost and thermal energy of the accreted matter is assumed to be radiated away. In some models, in order to suppress the $m = 1$ mode in the disk we restrict the motion of the BH and fix it at the disk center of mass.

4. RESULTS AND DISCUSSION

Globally unstable models of galactic disks with equal mass in the disk and in the halo (within 10 kpc) have been evolved in order to trigger the radial inflow. The models without star formation are labeled A and those with star formation, B. Within each set, the models differ only in the global gas mass fraction f_g, unless specified otherwise. We, therefore, denote a specific model by its generic name and the value of f_g taken as a percent. For example, A2.5 means a model without star formation which contains 2.5% gas.

4.1. *Galactic Disks Without Star Formation*

4.1.1. *Positions of Major Resonances in the Disk*

The stellar bar forms on a typical timescale of one to two disk rotations (see for example the evolution of the pure stellar model in Figure 3 of Shlosman & Noguchi 1993). When the bar instability enters the nonlinear regime and can be visually recognized, it already has a well-defined pattern speed Ω_b. Model A0 shows a $\lesssim 15\%$ decrease in Ω_b during its evolution of some $24\tau_{\rm dyn} \sim 1.2 \times 10^9$ yr. Models with the gas component exhibit a stable or slightly *increasing* Ω_b owing to the inflow of gas to the center, for at least as long as this inflow occurs. During the growth of the bar it rotates faster than max ($\Omega - \kappa/2$), where Ω and κ are the angular velocity and the epicyclic frequency of the stars in the disk, respectively. This does not allow for the existence of an inner Lindblad resonance (ILR) associated with the large-scale rotation curve of the galaxy and confirms our earlier calculations (Shlosman & Noguchi 1993; see also Sellwood 1981 and review by Athanassoula 1984). We note in passing that the bar length, $r_{\rm bar} \sim r_m$, is smaller than the distance to the corrotation resonance, $r_{\rm bar}/r_{\rm cor} \sim 0.6$ for model A0, although $r_{\rm bar}$ is ill-defined. For A10 this ratio is ~ 0.9. Corotation for a pure stellar disk is at $r_{\rm cor} \sim 9$ kpc and moves in for increasingly gas-rich disks, in accordance with a faster bar pattern speed mentioned above, e.g., $r_{\rm cor} \sim 6$ kpc for A10. The disk rotation curve is slightly modified after a couple of rotations as a result of stellar mass redistribution in the disk due to the gravitational interaction of the bar with the outer disk and the halo. Analysis of individual stellar orbits shows that the inner disk is losing its angular momentum as the circular stellar orbits become more radial causing disk mass to be more centrally concentrated. A single ILR associated with the central singularity is initially located well within 100 pc of the BH and moves out as the BH grows (for models with the gas).

The use of the linear theory to determine the existence of ILR(s) may be confusing in the presence of a strong stellar bar which provides a nonlinear bisymmetric perturbation. In the pure stellar case we measure the bar's strength (maximal ratio of nonaxisymmetric force to radial force) to be of the order of unity and an axial ratio of 4:1. For purely academic reasons, if linear analysis is applied by azimuthally averaging the mass distribution, the $\Omega - \kappa/2$ curve shows a weak maximum around ~ 400–500 pc from the center, which becomes more pronounced at the time of maximal gas inflow rate into the inner 1 kpc and the maximal accretion rate onto the BH. This shape, in principle, allows for one or two ILRs not associated with the BH. The orbit analysis performed below, however, exposes the limits of linear approximation. Models without the BH show a similar behavior, with the central gas concentration playing the role of the BH.

In order to understand the gas dynamics in the presence of a strong bar, we have performed a limited study of stellar orbits inside corotation. A more comprehensive analysis of stellar orbits (Contopoulos & Papayannopoulos 1980; Athanassoula et al. 1983; Sparke & Sellwood 1987; Pfenniger & Friedli 1991, and others) in two-dimensional and three-dimensional bars is in general agreement with our results. We have focused our attention on the principal families x_1, x_2, and x_3. The x_1 orbits which are aligned with the stellar bar for $r < r_{\rm cor}$ dominate most of the way to the center. In view of the rotating nonaxisymmetric background potential, only the Jacobi integral, $E_{\rm J} \equiv E - \boldsymbol{\Omega}_b \cdot \boldsymbol{L}$ (e.g., Binney & Tremaine 1987) is conserved along the orbit, where E and L are energy and angular momentum. Typically, x_1 are simple ellipse-like nonintersecting orbits, but they may develop end-loops which have grave consequences for the gas residing there (§§ 4.1.2 and 4.2). The x_2 orbits are aligned with the minor axis of the bar and confined between the ILRs. However, both x_2 and x_3 are absent in our case. Because there is no abrupt change from x_1 type of orbits to x_2 orbits, we conclude that no ILRs associated with the large-scale rotation curve in the disk exist during our numerical simulations (see also Athanassoula 1992a). This of course does not preclude the formation of ILR(s) during later evolution when the bar will slow down sufficiently by losing its angular momentum to the halo and the outer disk.

A more careful look at the x_1 orbits confined to the stellar bar during its growth reveals the following trend. We have constructed the characteristic diagram for this potential, i.e., Jacobi integral versus orbit crossing point to the short axis of the potential. Around $\tau \sim 4\tau_{\rm dyn}$, for a pure stellar model A0, the bar strength is below 0.2. The x_1 orbits have a low eccentricity up to some $E_{\rm J}$ which corresponds to the semimajor axis of ~ 7 kpc. Above this energy and up to corotation the x_1 develops end loops and bifurcates into diamond-shaped orbits which are cusped or possess end loops. At $\tau \sim 6\tau_{\rm dyn}$, the bar's strength is around 0.45, and the x_1 orbits become more eccentric. A region of looped x_1 orbits and their offsprings, diamond-shaped orbits cusped or with the end loops along the

bar axis, exists between ~7–9 kpc. Roughly, this is the region between the bar's semimajor axis and corotation. At $\tau \sim 8\tau_{dyn}$, we observe that the highly eccentric *and* cusped x_1 orbits end around ~7 kpc, while rectangular and diamond-shaped orbits with the end loops dominate the region up to corotation.

4.1.2. *Gas Flow in the Stellar Bar*

For gas-poor disks, with $f_g < 0.1$, the gas forms two leading shocks in response to the growing bisymmetrical perturbation. The shocks extend from ~1–2 kpc out to the corotation radius. They are initially curved but straighten out, recede toward the bar major axis (Fig. 3, between time $5–7\tau_{dyn}$), and weaken as the stellar bar becomes narrower. The gas, which is initially on almost circular orbits (maximal angular momentum at given energy) and goes through the shocks, is losing much of its rotational support and is progressively trapped by the bar potential. Our previous analysis of principal families of stellar orbits helps to understand this process. As the dominant periodic orbits between the end of the bar and corotation are all looped, they cannot sustain the gas. The latter shocks and falls inward accumulating at the highest Jacobi "energy" orbits without the end loops. Such orbits are found just inside the bar at ~6–7 kpc. However, as the stellar bar grows in strength the x_1 orbits become strongly eccentric and *cusped* at all radii inside r_{bar}. This cuspiness affects the gas close to the apocenters of its circulation in the bar as it excites shocks and drives the gas further inward, although not as violently as between r_{bar} and r_{cor}. Its consequences are more prominent when the gas does not fragment as, for example, when there is an energy injection by massive stars (see § 4.2).

The gas circulation (which we shall call a "ring" for brevity) in the bar is highly eccentric, with its semimajor axis initially being only slightly smaller than r_{bar} and is comparable to the velocity turnover radius r_m (as observed, for example, in the Seyfert 1 galaxy NGC 6860; see Lipari, Tsvetanov, & Macchetto 1993). When the gas ring within the bar has stabilized, the large-scale shocks are weak and only slightly offset (leading) from the bar's semimajor axis. Because the gas surface density of the ring is high in comparison with the background and the ring dominates the kinematics of the flow, we concentrate mainly on it. We note that simulations of steady state flows in weak bars do not report such rings (e.g., Athanassoula 1992b), which is consistent with our understanding of x_1 orbit shapes as discussed in § 4.1.1. Because we study gaseous response to the strong bar instability, we focus here on the initial few revolutions of the stellar bar *before* any steady state flow can be established (see also Friedli & Benz 1993). The latter is addressed in a separate paper (Shlosman & Heller 1993).

The growing surface density in the ring results in Jeans insta-

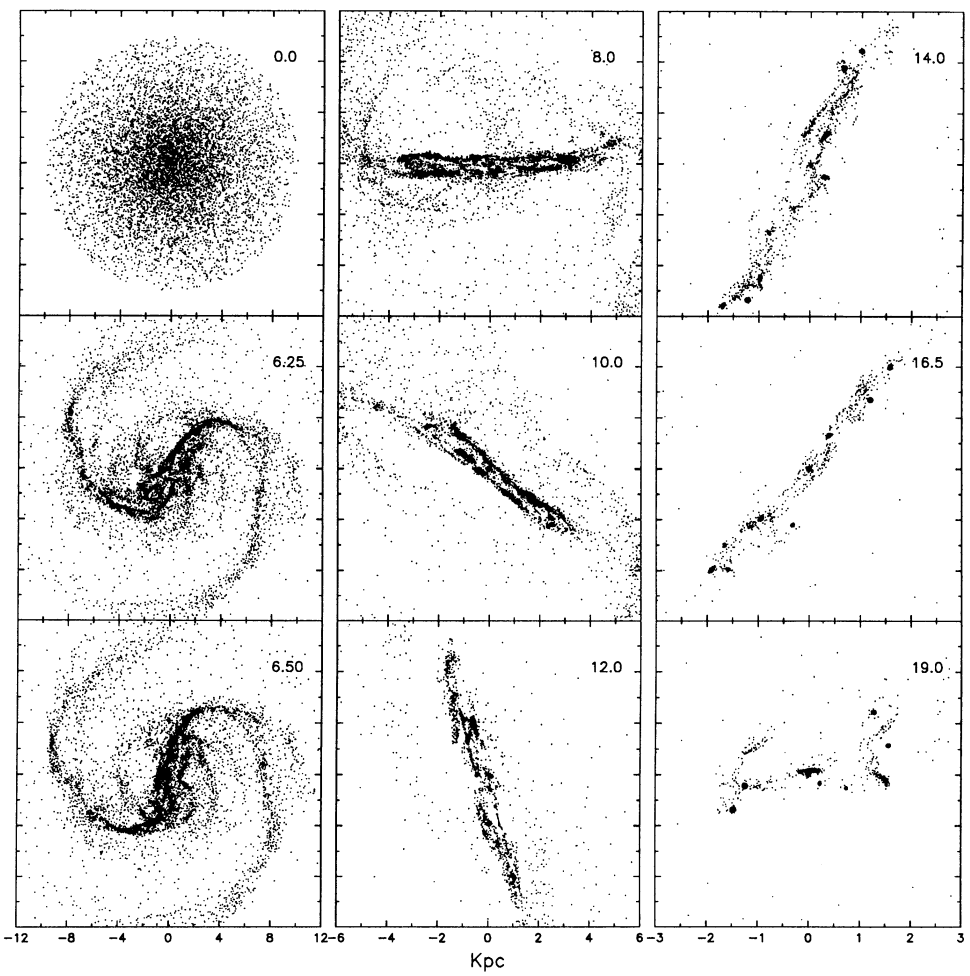

FIG. 3.—Evolution of gas in the globally unstable galactic disk of model A1 with 1% gas, a "seed" BH (*asterisk*), and no star formation, seen face-on. The time in units of τ_{dyn} is given in upper right corners. The frames are 24 kpc, 12 kpc, and 6 kpc in the left, middle, and right columns. The final $M_{BH} \sim 6 \times 10^8 M_\odot$.

bility which triggers its fragmentation. The developing inhomogeneities lead to nonuniformity in the velocity field and to internal shocks which in turn compress the gas and increase its self-gravity. Contrary to stars, the gas cannot populate intersecting orbits. This creates shocks in the supersonic flow causing the gas streamlines to experience discontinuities. Reflection shocks are clearly visible in and around the ring and contribute greatly to the internal dissipation and clumping which increases dramatically with f_g. The fragments stay within the ring and affect the flow downstream; the circulation pattern is constantly disrupted and reformed, which is associated with the additional loss of angular momentum (model A1 shows a typical behavior for this range of f_g, see Fig. 3). The above processes frequently destroy the bisymmetry in the gas (including the shape of the ring), despite the barlike nature of the underlying stellar gravitational potential which persists at all times. These and other distortions in the gas distribution relative to the bar major axis lead to a gravitational torque on the gas by the bar and to the inflow.

The strongest inflow in the gas-poor disks is first observed on scales of ~ 3–6 kpc (between $\tau \sim 6$–$13\tau_{\rm dyn}$), while the inflow on smaller scales of ~ 1 kpc picks up around $\tau \sim 12$–$14\tau_{\rm dyn}$. This delay is related to the loss of angular momentum by the eccentric ring. The cuspiness of x_1 orbits at the apocenters has a most dramatic effect on the gas by inducing shocks there. Consequently, the gas response appears first at the apocenters of the flow where large gaps open immediately (e.g., Fig. 3, at $\tau \sim 8$–$10\tau_{\rm dyn}$). A few gravitationally bound gaseous blobs (knots), ~ 10, are visible along the ring whose semimajor axis is gradually shrinking from the initial ~ 5–6 kpc to ~ 2 kpc due to gravitational interaction between these blobs and dissipation in the gas. Additional material is fed to the ring along the stellar bar at a typical inflow velocity of 100 km s^{-1}. The velocity of the gas in the ring is a strong function of the orbital phase angle; because the flow is highly eccentric, its streaming velocity of ~ 90–130 km s^{-1} is a large fraction of the local virial velocity at the pericenter and is negligible (in the stellar bar frame) at large distance from the center. It is important to emphasize that the streaming velocity in the ring in no way represents the inflow velocity to the center. The latter is associated with the secular evolution of the ring. The softened gravity (at 75 pc for models without star formation) prevents the blobs from further fragmenting. These blobs experience frequent collisions and gravitational interactions among themselves but nevertheless tend to preserve their number, although some are tidally disrupted, fragment, or merge. Around $\tau \sim 13$–$14\tau_{\rm dyn}$ the semimajor axis of the eccentric ring starts to shrink at an accelerated rate, by a factor of ~ 2 in ~ 3–$4\tau_{\rm dyn}$. At this point the shape of the ring becomes heavily distored, it quickly loses its angular momentum and the clouds are dumped in the vicinity of the BH. All of the above processes are sped up with increasing f_g. The fate of this gas is discussed in § 4.3.

For gas-rich models, with $f_g \gtrsim 0.1$, the local gravitational instabilities in the gas prevent the formation of large-scale shocks due to the disruption of the flow pattern by the massive self-gravitating fragments within the corotation radius. The gaseous ring which is so prominent for $f_g < 0.1$ is replaced by a number of these fragments. Model A10 shows the subsequent evolution of the gas distribution (Fig. 4). This regime has been studied in detail by Shlosman & Noguchi (1993) both analytically and using the "sticky" particle + TREE code. Present results based on SPH code support our previous calculations. The gaseous clumps experience dynamical friction with the background stellar disk (due to the asymmetric drift), lose their angular momentum, and spiral in. The dynamical effect of the halo in the vicinity of $r_e \sim 3$ kpc in the disk is almost two orders of magnitude weaker, assuming that the halo is axially symmetric. The latter is a valid approximation because the stellar bar does *not* form in this regime. To verify that the dynamical friction is indeed responsible for the inflow, we have frozen the background stellar potential. As a result, stars have not been able to respond to gravitational perturbations by the gas clumps, and wakes did not form behind them. The inflow rates, therefore, have been reduced by a factor of a few.

The dynamical friction is very efficient in heating the stellar "fluid" on the disk rotation timescale. Hot stellar disks are much less susceptible to global instabilities. Scattering by massive clumps and other inhomogeneities prevents the formation of a strong bar. Instead, a short and an almost unrecognizable oval forms for $f_g \sim 0.1$. For even higher f_g, the bar disappears without a trace, and the disk is stabilized against a bar instability. Based on these results, Shlosman & Noguchi (1993) gave a semiempirical estimate of the domain of global stability for different halo-to-disk mass ratios of a two-component self-gravitating disk.

The above models represent a limiting case for both the evolution of the gas distribution and its effect on the global stability of the stellar disk. This is mainly because of neglecting the main heating mechanism in the ISM—the energy input by massive stars and supernovae. Under these conditions, the gas is subject to Jeans instabilities and, therefore to the extreme clumpiness. Although this may be related to the formation of giant molecular clouds (GMCs) and giant molecular associations (GMAs), the latter have a limited lifetime due to the star formation and subsequent disruption by stellar winds and supernovae remnants. As we shall see in § 4.3, this is especially true for the gasdynamics of the central 1–2 kpc (series A models) which are dominated by a few massive clumps that have grown at the expense of low-mass clouds. These models can be used for comparison with more complex models which involve heating by massive stars.

4.2. *Galactic Disks With Star Formation*

The development of the stellar bar instability (and the gasdynamics prior to bar formation) in the gas-poor models is unaffected by the introduction of star formation. The evolution bifurcates with the appearance of large-scale shocks which produce compression $\sim M^2$, the Mach number in the flow, because of the isothermal equation of state adopted for the gas. Increased surface density in the gas induces fragmentation and local gravitational collapse. The resulting star formation acts as a *negative* feedback on the ISM by depositing $\sim \xi$ of the energy release by OB stars and supernovae and limiting the growth of inhomogeneities. Therefore, the duration of a local star formation event is of the order of the clump dispersal time.

The parameters of the eccentric "ring," which forms after one rotation period of the disk, are similar to those in models without star formation. The ring, however, has a much less clumpy mass distribution and does not fragment, avoiding the formation of large gravitationally bound clumps (e.g., model B1 in Fig. 5). The ring's cross section is defined by competition between internal dissipation and energy injection by massive stars on the one side and the self-gravity in the gas on the other side. It is unrelated to the gravitational softening which is fully dynamic for the gas on all scales and limitless for models with star formation. If the cross section would be determined by the

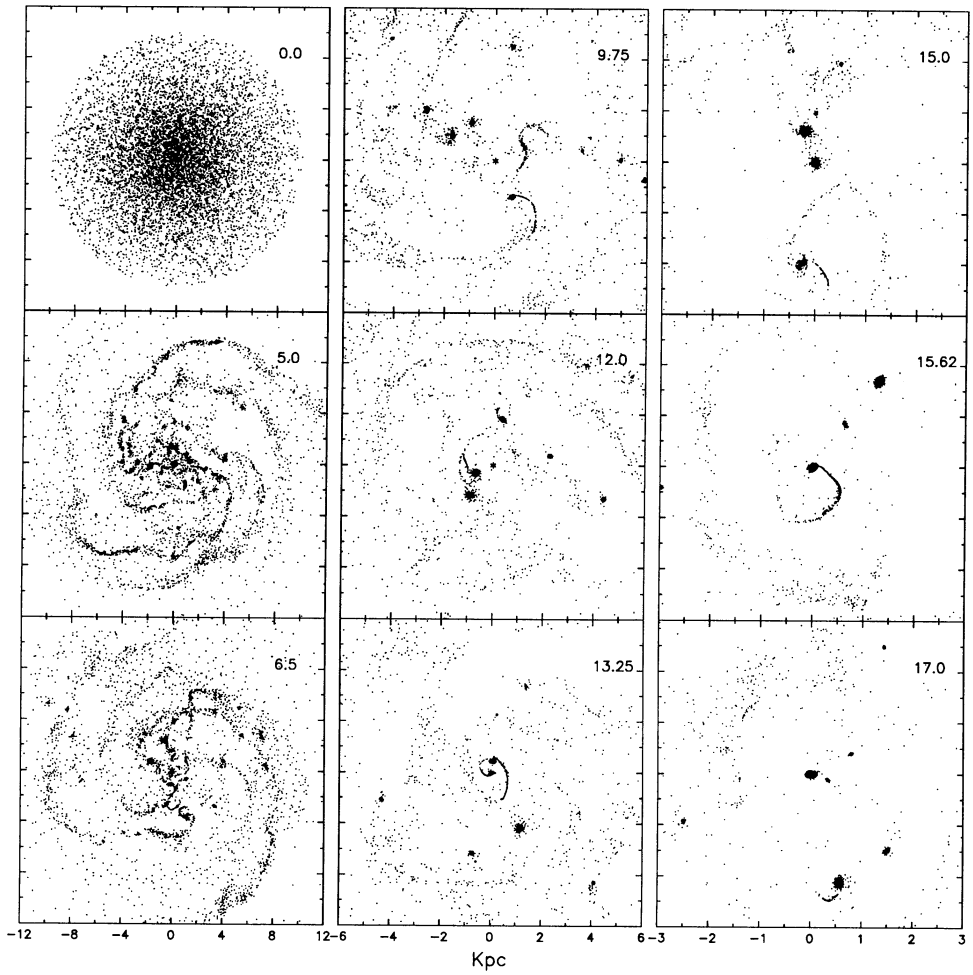

FIG. 4.—Evolution of gas in the globally unstable galactic disk of the model A10 with 10% gas, a "seed" BH (*asterisk*), and no star formation, seen face-on. The time in units of τ_{dyn} is given in upper right corners. The frames are 24 kpc, 12 kpc, and 6 kpc in the left, middle, and right columns. The final $M_{BH} \sim 2.5 \times 10^9 M_\odot$.

softening (or smoothing), the ring would respond by shrinking until the internal pressure gradient (with or without energy injection) would stabilize it. Star formation is concentrated in regions where the inflow along the stellar bar feeds the ring, as shown on the star formation map for models B1 and B10 (Figs. 6*a* and 6*b*). In addition, star formation is prominent within the inner few hundred parsecs from the center, where small-scale shocks are clearly visible and where the flow is generally more compressed. The sites of the most intense star formation frequently disrupt the flow pattern in their vicinities. The ring, however, appears to be very robust and reforms shortly thereafter.

As we have mentioned before, the gas initially accumulates at the maximal Jacobi "energy" x_1 periodic orbits without end loops and forms an eccentric "ring" there. Both inhomogeneities and energy injected by massive stars perturb these orbits and lead to the thickening of the ring and shocks in the flow. As the ring evolves, first shrinking along its minor axis, the Kelvin-Helmholtz (K-H) instability develops along the ring's major axis, close to the pericenter where the flow velocities are opposite and maximal, creating considerable shear. No such effect was observed for A models, as the flow there is highly fragmented. However, conditions in B models are particularly favorable for the "runaway" mixing between two layers forming vortices which dissipate the gas kinetic energy. We seriously doubt whether this mechanism can compete with the gravitational torques on the gas in forcing it inwards. This is based on our analysis of the angular momentum loss rate (transfer) in the gas. The latter does not show any substantial change in slope when the K-H instability is operating. We estimate that nongravitational torques contribute less than $\sim 10\%$ to the overall angular momentum loss by the gas in the ring. In addition, as we discuss in § 4.5, the numerical scheme will probably underestimate the timescale of energy dissipation due to this instability, and a careful study should precede any claim for a quantitative effect.

In model B1, the elliptical ring halves its major axis in approximately one disk rotation time (Fig. 5 at $\tau \sim 9$–$15\tau_{dyn}$; this takes even less time for B2.5 to B10 model sequences) and then quickly, in $\sim \tau_{dyn}$, dumps its material at the center, going through a number of radial pulsations. The peak of star formation and the maximal inflow rate into the inner kpc correspond to this moment. As its end-product it forms a ~ 0.5–1 kpc-size disk whose properties we discuss in the next section. Such a short timescale, a few $\times \sim 10^7$ yr, requires inflow velocities to be a large fraction of the local free-fall velocity, ~ 200 km s^{-1}. We measure velocities in the 100–150 km s^{-1} range during this narrow time interval. The inflow rate into the inner kpc is not monotonic but builds up a large amplitude variability. The rate of star formation shows similar "burst" behavior with

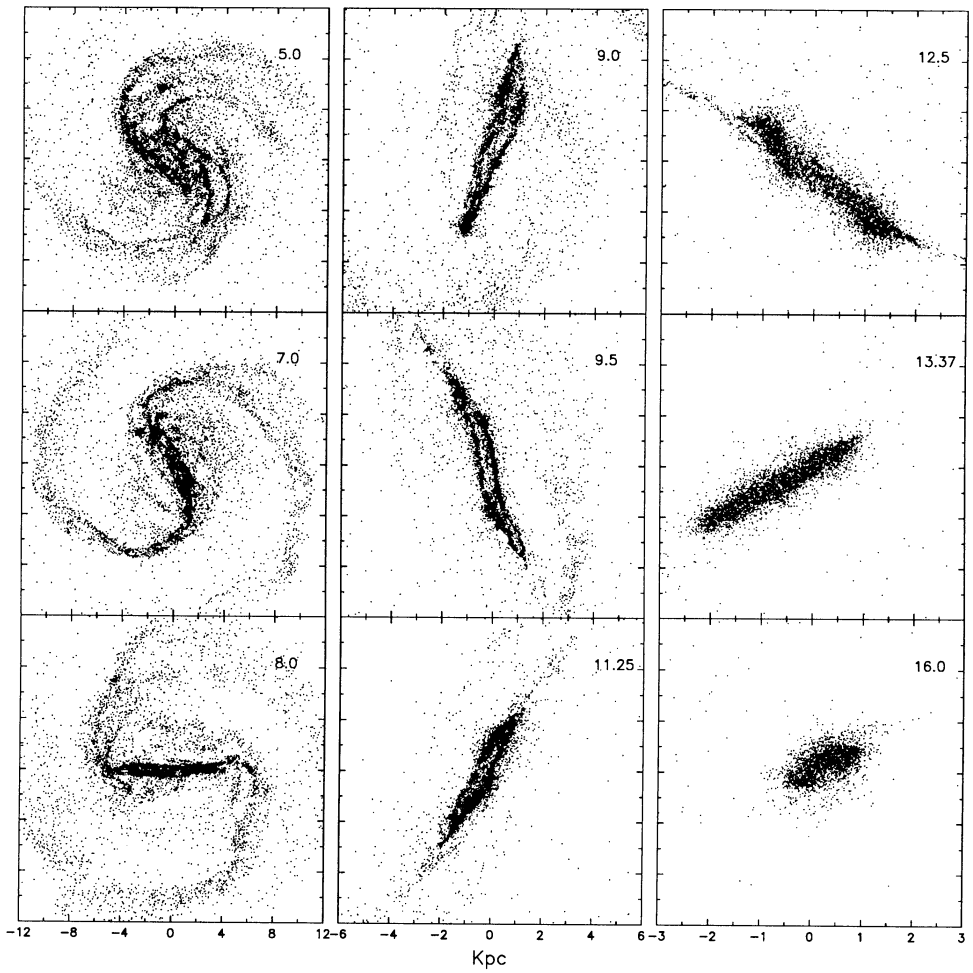

FIG. 5.—Evolution of gas in the globally unstable galactic disk model B1 with 1% gas, a "seed" BH (*asterisk*), and star formation ($\xi = 0.05$), seen face-on. The time in units of τ_{dyn} is given in upper right corners. The frames are 24 kpc, 12 kpc, and 6 kpc in the left, middle, and right columns. The final $M_{BH} \sim 6 \times 10^8\ M_\odot$.

increasing amplitude. Both phenomena exhibit a degree of temporal correlation, as can be seen in Figure 7*a*, and most likely are casually related. The pulsational overstability of the gaseous ring is excited by positive feedback from the OB star and supernovae energy release, causing a catastrophic loss of kinetic energy in the ring. The starburst timescale is short, ~ 0.2–$0.5\tau_{dyn} \sim 1$–2.5×10^7 yr, and the bursts are separated by $\sim \tau_{dyn}$ long periods of relatively low star-formation activity. This type of behavior is well described by a simple mathematical model advanced by Scalo & Struck-Marcell (1986).

The star formation seems to induce an additional loss of angular momentum in the gaseous ring. This phenomenon is related to increased mixing of the ISM due to the stirring effect by the OB stars and supernovae concentrated at the ends of the major axis of the ring. A fraction of the gas is expelled in this way from the ring. The inflow rates toward the inner kiloparsec calculated above, however, must be taken with caution. Our neglect of low-mass star formation and the uncertainty in the dissipation timescale of turbulent eddies must contribute to the overestimate of these rates.

A comparison between models of gas-rich disks, with and without star formation (models A10 and B10; see Figs. 4 and 8), shows explicitly the effect of dynamical heating by the inhomogeneities in the gas. Because all stellar particles have equal masses (as well as all SPH particles), the particle density is directly proportional to the mass density. The lower density contrast, which is maintained in the gas when star formation is active, provides less damping of the bar instability. As a result, the stellar bar is more prominent in the model B10 than in A10. Contrary to the evolution of gas-rich A models, the gaseous ring is clearly forming in model B10 and even in B15. In all cases the subsequent evolution is fast, and the gas quickly falls to the center forming a ~ 0.5–1 kpc radius disk. This disk continues to accumulate mass, and, if the cooling prevails over the heating by star formation, it develops a multiarm spiral structure.

4.3. *Gas Dynamics of Inner Kiloparsec and the Growth of Central BH*

Star formation profoundly alters the evolution of the gas distribution in the inner disk. Although A and B series of models have identical initial conditions, the dynamic state of the gas in the inner 1 kpc exhibits very little similarity. In the models without star formation, all the gas in this region is essentially concentrated in a few clumps which are distributed in a flattened disk configuration and have masses that are a steep function of f_g (Shlosman & Noguchi 1993). The intercloud medium is either accreted by the BH or expelled to larger radii by the tidal torques of these massive objects, which excite strong density waves within ~ 2 kpc. The gas clumps populate

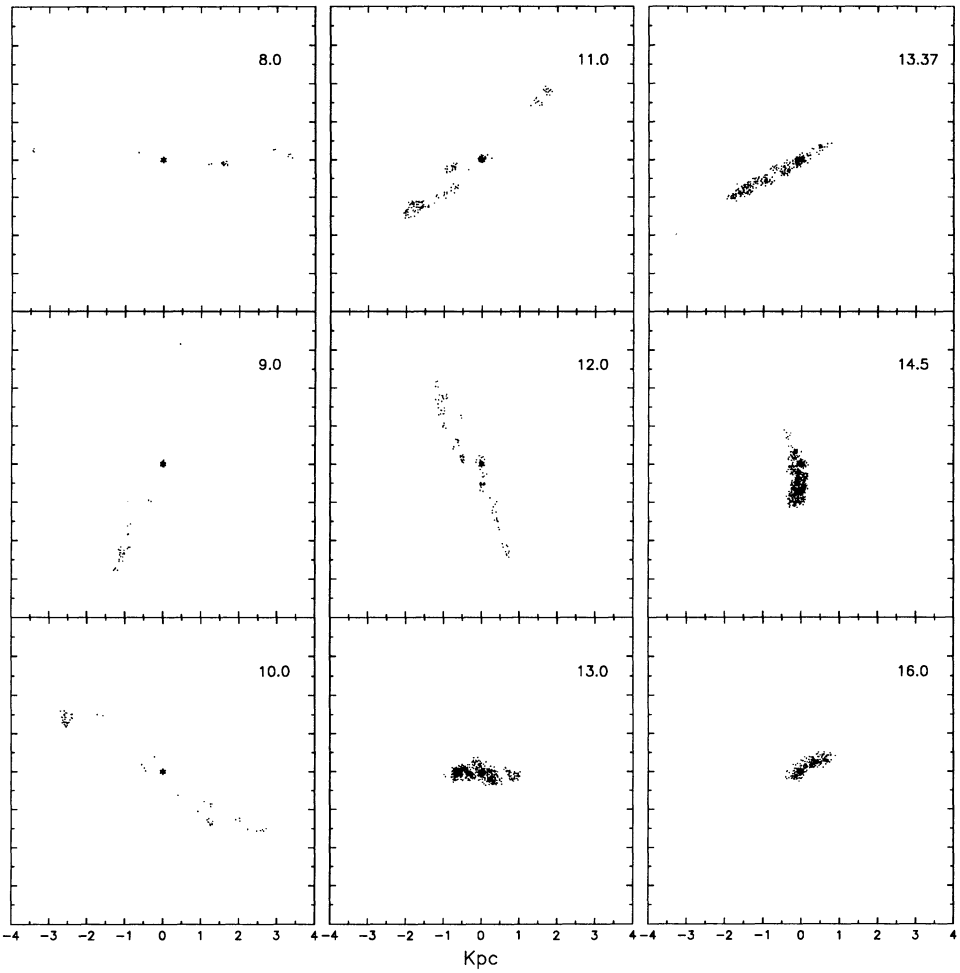

FIG. 6a

FIG. 6.—(*a*) Star formation map for the model B1 with 1% gas, a "seed" BH (*asterisk*), and $\xi = 0.05$. The time in units of τ_{dyn} is given in upper right corners. The frames are 8 kpc. (*b*) Star formation map for the model B10 with 10% gas, a "seed" BH (*asterisk*), and $\xi = 0.05$. The time in units of τ_{dyn} is given in upper right corners. The frames are 8 kpc.

orbits which occasionally take them close to the BH. The clumps are then tidally disrupted, and some fragments are captured by the hole, forming disks with radii $\sim$60–80 pc. This radius is related to the limiting gravitational softening in the models without star formation and should impede further fragmentation. The evolution of these disks is outside the scope of this paper. The BH is also able to scatter some of the clouds into orbits with *negative* angular momentum, and occasionally *most* of the material within the inner 1 kpc counter-rotates.

Series B models (with star formation and the "seed" BH) always form nuclear disks within the inner kpc as a result of dumping of the bar material at the center (discussed in § 4.2). These disks rotate with Keplerian velocities of ~ 100 km s^{-1} at ~ 500 pc, which implies a typical mass of $\sim 10^9\ M_\odot$ within this radius. Their surface density profile is quite flat, which means that most of the mass is residing at larger radii, giving the impression of a ring. Following the formation of these disks, the star-formation rate declines, allowing the disk to rapidly cool down and contract along its rotation axis. It becomes geometrically thin and mildly self-gravitating. Efficient cooling drives spiral structure in these disks and the whole configuration resembles nuclear regions of hot-spot galaxies (e.g., NGC 4314; see Wakamatsu & Nishida 1980; Garcia-Barreto et al. 1991). The decline in star-formation activity is clearly associated with the peak accretion rate onto the BH (Fig. 7b). The amount of gas in the neighborhood of the BH decreases and so does its dynamical importance. We find that catastrophic growth of the BH occurs when the ratio of the gas mass to the total mass of gas, stars, and halo combined within 1 kpc reach $\sim$20%–30%. All series B models experience such growth, while only gas-rich series A models show this behavior. The peak luminosity of the OB stars in the disk range between ~ 2–8×10^{45} ergs s^{-1} for $f_g \simeq 0.01$–0.15.

Both series of models are characterized by a strong inflow within $\sim$5–6 kpc radius, with the *median* rates at $r = 1$ kpc shown in Figure 9*a*. Series B models have inflow rates higher by a factor of < 3 for the gas-poor disks, and lower rates for the gas-rich ones. For all models there is initially about 5% of the total gas mass within the inner kpc. As a result of the radial redistribution, a substantial fraction of this gas moves inwards (Fig. 9*b*). Between 50%–90% of this gas is accreted by the central BH during this phase. *Median* accretion rates are shown in Figure 9*c* and represent an inflow across the "accretion" radius of 20 pc. The overall impression is that the

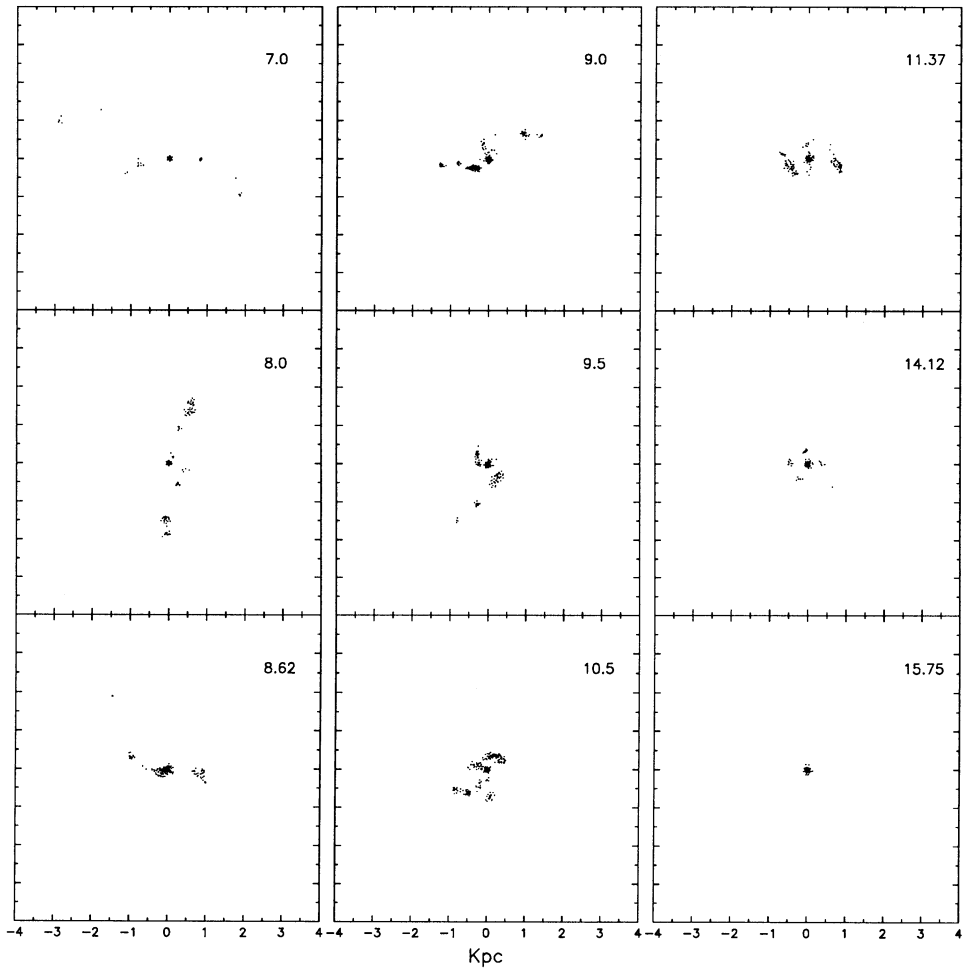

FIG. 6*b*

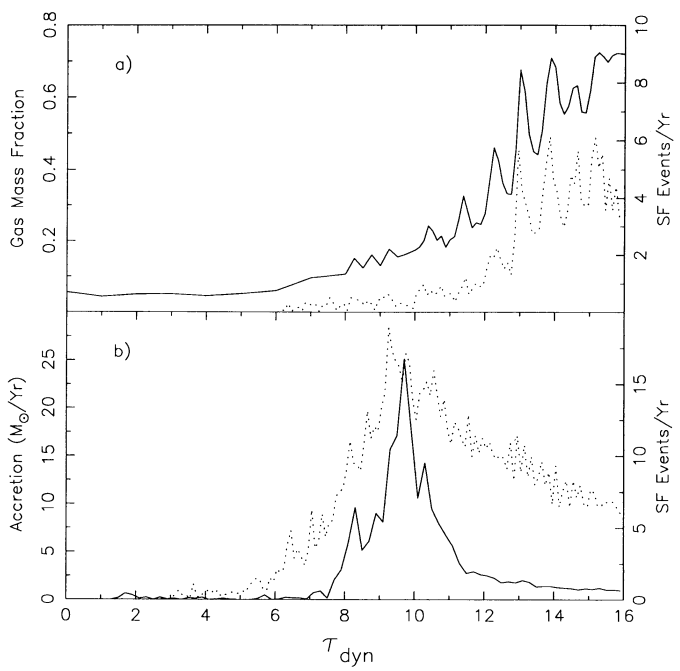

FIG. 7.—(*a*) Correlation between star formation rate (*dotted line*) and the fraction of the gas (*solid line*) in the inner 1 kpc for model B1. The right vertical axis gives the rate of massive star formation per year. The shape of the inflow rate curve (omitted) closely follows the solid line. (*b*) Correlation between star formation rate (*dotted line*) and accretion rate onto the BH (*solid line*) for the model B5.

gas-poor models A and B exhibit a surprisingly similar behavior regarding the parameters displayed in Figure 9, while the gas-rich models show a diverging trend.

For A models, the actual inflow towards the 1 kpc region and the accretion onto the BH are characterized by a large dispersion around the median rates. Both are rather sporadic, with extended dormant periods that are followed by relatively short periods of activity. It is the inhomogeneity of the ISM, which is much stronger in the A models, that this responsible for this type of behavior. As we have mentioned earlier, neglecting star formation prolongs the lifetime of self-gravitating clumps which otherwise would be dispersed by the energy input from OB stars and supernovae. Therefore, mass accretion onto the BH is dominated by rare events which represent the capture of a passing cloud—a process that is enhanced by the presence of two to three massive clouds in the neighborhood of the BH. These clouds experience complicated motions with an amplitude of up to 2 kpc. The *peak* accretion

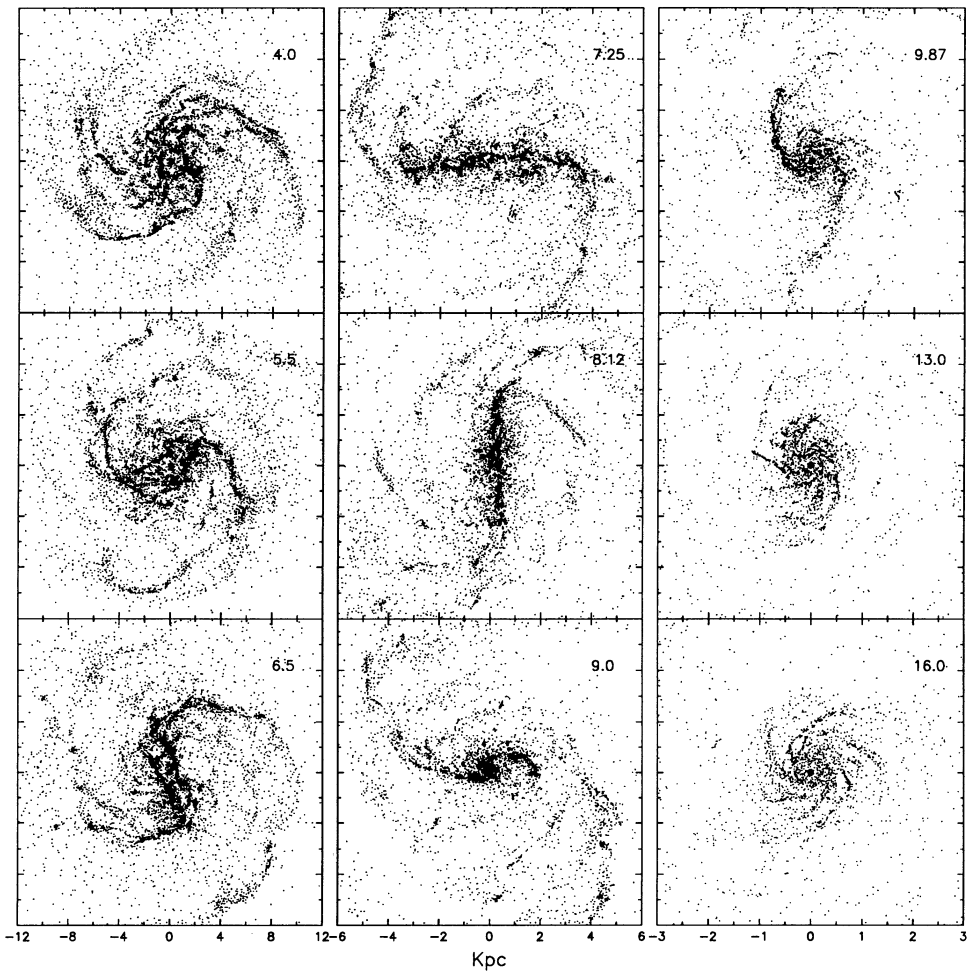

FIG. 8.—Evolution of gas in the globally unstable galactic disk model B10 with 10% gas, a "seed" BH (*asterisk*), and star formation ($\xi = 0.05$), seen face-on. The time in units of τ_{dyn} is given in upper right corners. The frames are 24 kpc, 12 kpc, and 6 kpc in the left, middle, and right columns. The final $M_{BH} \sim 2.8 \times 10^9\ M_\odot$.

rate may exceed the median rate by a factor of 10 and 6 for A and B models, respectively. Thus, the gasdynamics in the inner kpc is essentially a fewbody problem for the models without star formation. Clumps experience gravitational interactions that frequently result in mergers. Tidal disruptions lead to the formation of narrow bridges which fragment giving birth to clouds with a broad mass spectrum. The dynamic softening we have incorporated is crucial in allowing the formation of clumps dense enough to withstand these tidal interactions (Fig. 4).

To study the formation of a central concentration which possibly evolves toward a BH, we have rerun the A10 and B10 models (Figs. 10 and 11, respectively) in the absence of the "seed" BH (these are labeled with *N*). The large-scale evolution is not affected by this modification. However, the inner kiloparsec is clearly different. We first address the models without star formation. In models A10 and A10N we observe the formation of a massive binary cloud system with an initial separation of around 0.7–1 kpc, surrounded by a few less massive clouds. In A10 such a pair (which is positioned off-center) is quickly disrupted by the BH which captures and digests one of its members. In A10N the evolution is slower but is clearly pointing toward the formation of a single massive object which grows at the expense of its less massive neighbors and at the same time damps its motion, approaching the center of mass of the disk + halo system. This difference is understandable because in A10N there is no rigidly fixed (to the disk center of mass) BH which absorbs part of the momentum. If the BH is released (unfrozen), it experiences a random walk with an amplitude of about a few hundred parsecs, and further evolution follows that of A10N. The persistent formation of massive binary clouds at the center raises an interesting possibility of a binary BH. This outcome depends of course on the orbital versus internal evolution of large molecular clouds. When sufficiently massive BHs form before the clouds merge, their subsequent orbital evolution can be prolonged up to 10^{10} yr if they remain on circular orbits (Begelman, Blandford, & Rees 1980). However, this timescale will be sharply reduced for elliptical orbits, as we observe in our simulations.

Model B10N with star formation and no "seed" BH shows a different pattern of "starburst" activity within the inner 1 kpc as compared to model B10. In particular, the star formation rate monotonically increases up to time $\sim 16\tau_{dyn}$ instead of peaking at the time of nuclear disk formation at ~ 9–$10\tau_{dyn}$. This results in extensive heating and thickening of the nuclear disk, which is substantially supported by both the gas pressure and rotation against the gravity. An observational counterpart of such a thick disk may have been recently detected (in H I absorption) in the form of a molecular torus with a radius of 500 pc in starburst galaxy NGC 1808 (Koribalski, Dickey, &

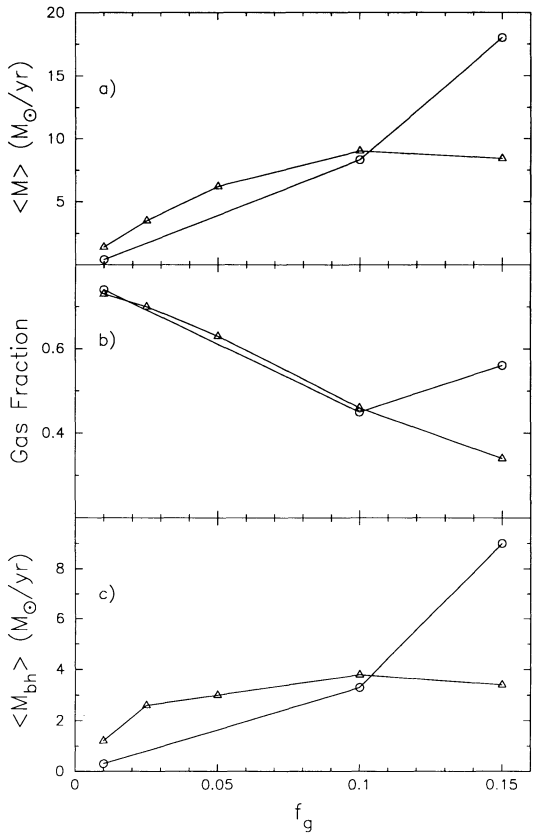

FIG. 9.—(*a*) Median inflow rates measured at $r = 1$ kpc for A (*circles*) and B (*triangles*) series as a function of gas fraction f_g. (*b*) Fraction of the total gas residing within the inner 1 kpc at the end of the simulation of A (*circles*) and B (*triangles*) series as a function of f_g. Mass of the BH is *included* in the gas mass. (*c*) Median accretion rates onto the BH for A (*circles*) and B (*triangles*) series as a function of f_g.

Mebold 1993). The pressure support stabilizes the disk against global instabilities and the gas mass accounts for $\sim 50\%$ of the total mass within 500 pc at the time $\tau = 13\tau_{dyn}$. Dynamically, the gaseous disk is a separate entity, i.e., dominated by self-gravity. It has an exponential density profile and solid body rotation. The semi-empirical global stability parameter t (e.g., Binney & Tremaine 1987), defined as the ratio of rotational kinetic energy to self-gravitational energy, is approximately 0.09 in the nuclear disk.

4.4. *Gaseous Bars in Nuclear Disks*

Fat nuclear disks seem to be the by-products of the radial redistribution of gas in our models with star formation and without the "seed" BH. They are massive and dynamically significant accounting for about one-half of the total mass within their radius of ~ 0.5 kpc and for $\gtrsim 40\%$ of the initial gas content of the galaxy. Therefore, it is natural to investigate their gravitational stability in the absence of additional complicating factors, such as star formation and a preexisting supermassive BH. To our knowledge, the study of the nonlinear evolution of self-gravitating gaseous disks has been limited to the stability of uniformly rotating incompressible fluids (e.g., Chandrasekhar 1969). Recently, Goodman & Narayan (1988) investigated the effects of self-gravity on incompressible shearing tori and Christodoulou & Narayan (1992) addressed the evolution of two-dimensional compressible self-gravitating annuli.

To simplify the problem of initial conditions and without claiming a comprehensive analysis, we take a nuclear disk composed of stars and gas from the model B10N at $\tau = 13\tau_{dyn}$ and follow its evolution *without* energy input by massive stars. The stars, which belong to the galactic disk, have a much larger velocity dispersion and vertical scale height than the gas, and, therefore, their effect on the gas is marginal. The stabilizing effect of the gas pressure is seen explicitly when the star formation is switched off—the disk rapidly cools down and collapses along the rotation axis. Initially nearly axisymmetric, the disk quickly develops a barlike mode which is clearly visible because most of the mass in the disk is locked up in the *gaseous* bar. In fact, shocks form along the bar affecting the gas flow in a way which closely resembles the gas flow in the large-scale stellar bar described in section 4.1. The growth of an $m = 2$ mode is confirmed by Fourier analysis, which also reveals that the $m = 1$ mode has a nonzero amplitude (the gaseous bar is off-center) as well as $m = 3$ and 4 modes which reflect the growing clumpiness. In addition, we observe the formation of density peaks whose growth is followed by the development of connecting filaments.

The further evolution is sensitive to the minimal softening length for gravitational interactions in the gas, ϵ_{min} (which we introduce for all models *without* star formation), because the size of the system becomes comparable with ϵ_{min} (see § 3.2). For higher resolution, and in order not to suppress possible instabilities, we have used $\epsilon_{min} = 7.5$ pc in this model, which is small compared with the system size of ~ 500 pc (model B10Na; see Fig. 12*a*). A comparison model with the "usual" $\epsilon_{min} = 75$ pc was also advanced (model B10Nb; see Fig. 12*b*), and the differences in the final product are discussed below.

In model B10Na, an eccentric ring results when $t \equiv T/|W| \sim 0.13 \pm 0.01$ (the error follows from our time resolution). The parameter t is measured now for the sphere encompassing the initial nuclear disk (radius 500 pc). It grows in mass and the inhomogeneities become more pronounced, especially at the opposite ends of the major axis where the flow slows down and two massive blobs feed on the rest of the material in the ring. At the early stage, the mass ratio of the gaseous ring to the total amount of gas + stars + halo particles in the sphere encircled by the ring is roughly ~ 1. The pattern speed of the distorted ring (in units of circulation frequency in the ring) is $\Omega_p/\Omega_r \sim 0.6$. The ring collapses along its minor axis and disappears. At some point, when $t \sim 0.24 \pm 0.02$, the gaseous bar fragments and the fragments increase their separation by a factor of 2 immediately following the breakup. This fission is the result of both the growth of the bar mode and the local gravitational instability in the gas. Lower velocities at the apocenter of the flow (at the bar ends) induce the Jeans instability there. It is a nearly symmetric fission (mass ratio of fragments 2:1) because most of the bar mass is now found in two massive blobs that formed at the opposite bar ends (Fig. 12*a* at $\tau = 13.08\tau_{dyn}$). Some gas, $\sim 20\%$, remains in a "diffuse" state in the region. Almost immediately, each of the two massive fragments experience fission as well. This hierarchical fission does not extend to a third generation. Instead, the two inner remnants form a binary system with an initial separation of ~ 300 pc and account for $\sim 40\%$ of the gas in the nuclear disk. The outer remnants are tidally disrupted and form a pair of trailing tails around the binary. Smaller fragments either merge with the two dominant masses or move

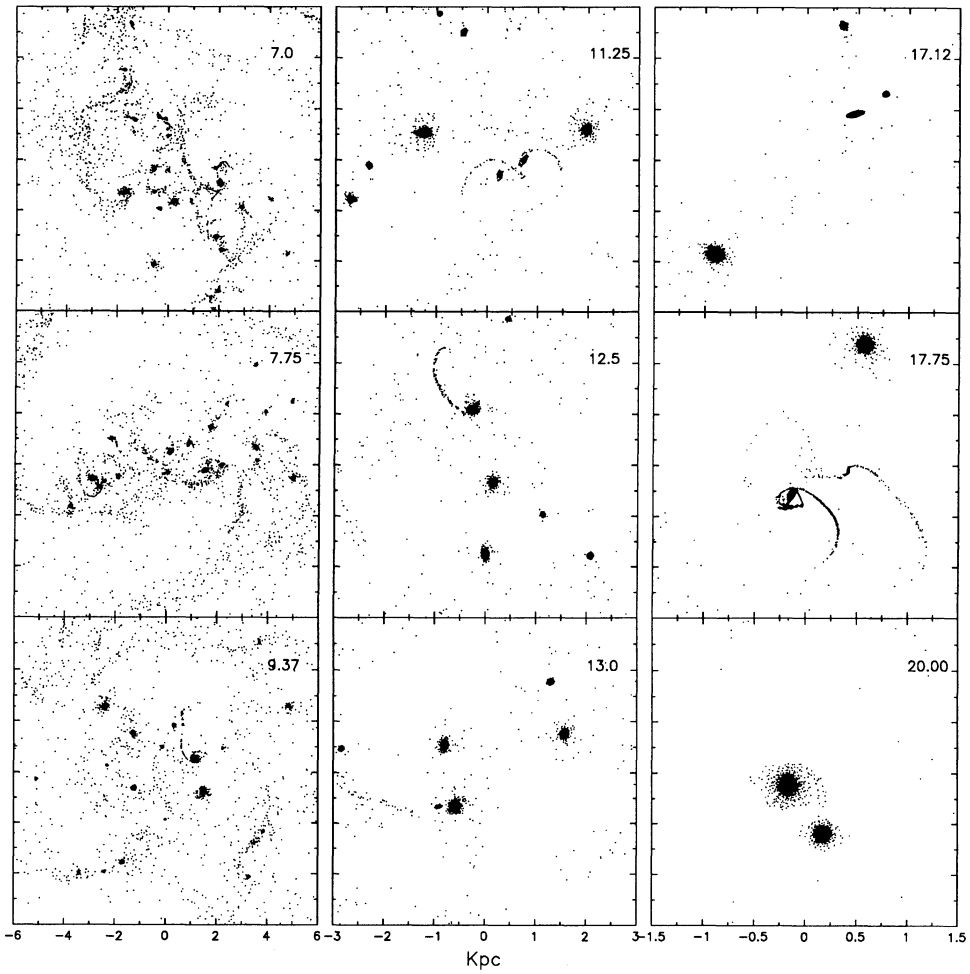

FIG. 10.—Evolution of gas in the globally unstable galactic disk model A10N with 10% gas, no "seed" BH, and no star formation, seen face-on. The time in units of τ_{dyn} is given in upper right corners. The frames are 12 kpc, 6 kpc, and 2 kpc in the left, middle, and right columns. The final mass of the central cloud is $\sim 4 \times 10^9 M_\odot$.

out to larger distances, carrying away most of the angular momentum. The massive binary quickly loses its orbital angular momentum and merges into a single massive object with a mass of $\sim 3 \times 10^9 M_\odot$ in a few $\times 10^7$ yr.

At an early stage, the evolution of a nuclear gaseous disk can be approximated by a sequence of Maclaurin spheroids (e.g., Chandrasekhar 1969) with increasing ellipticity. These are characterized by a constant density and a solid body rotation. Our disks rotate with a constant $\Omega(r)$ but have exponential density profiles. Maclaurin spheroids experience a secular instability at $t \sim 0.14$ and a dynamical instability (bar formation) at $t = 0.2738$. Their two-dimensional analogs, Maclaurin disks, are slightly less stable and form a bar already at $t = 0.25$ (Hunter 1963). We note that the fission experienced by the gaseous bar in our model may be genetically related to the dynamic instability of Maclaurin disks and spheroids and the near equality of critical t-parameters is not an accidental one.

We also find many similarities between the evolution of our nuclear disks and that of self-gravitating annuli studied by Christodoulou & Narayan (1992) in a two-dimensional analysis. Although their numerical models have much lower spatial resolution and idealized initial conditions, we confirm their results in the case of a self-gravitating annulus around a central object (their model 2; the central object corresponds to the mass encircled by the ring). Given the fact that we do not start with the ideal initial conditions, the ratio $\Omega_p/\Omega_r \sim 0.6$ which we measure prior to the fission is in excellent agreement with both the theoretical value 0.5 and numerical results of Christodoulou & Narayan. However, our higher resolution simulations show a more complicated behavior than just a fission into nearly equal mass fragments, as we are able to follow the evolution deep into the nonlinear regime.

If ϵ_{min} is kept at 75 pc (model B10Nb), the fission of the gaseous bar is not observed. The initial density peaks are smeared out and the bar becomes homogeneous with a sharp boundary. Transient shocks are visible and the bar evolves largely in a self-similar fashion by shrinking its size and driving an inflow over a period of one rotation $\sim 0.3\tau_{dyn} \sim 2 \times 10^7$ yr, as was argued by Shlosman, Begelman, & Frank (1990). At this stage the gas begins to completely dominate the gravitational field as it now comprises more than 90% of the mass within its radius. Fourier analysis shows that the $m = 2$ mode periodically grows and damps, which is also seen in Fig. 12*b*. When the bar semimajor axis becomes ~ 150 pc, the instability is damped by the softened gravity and the inflow slows down.

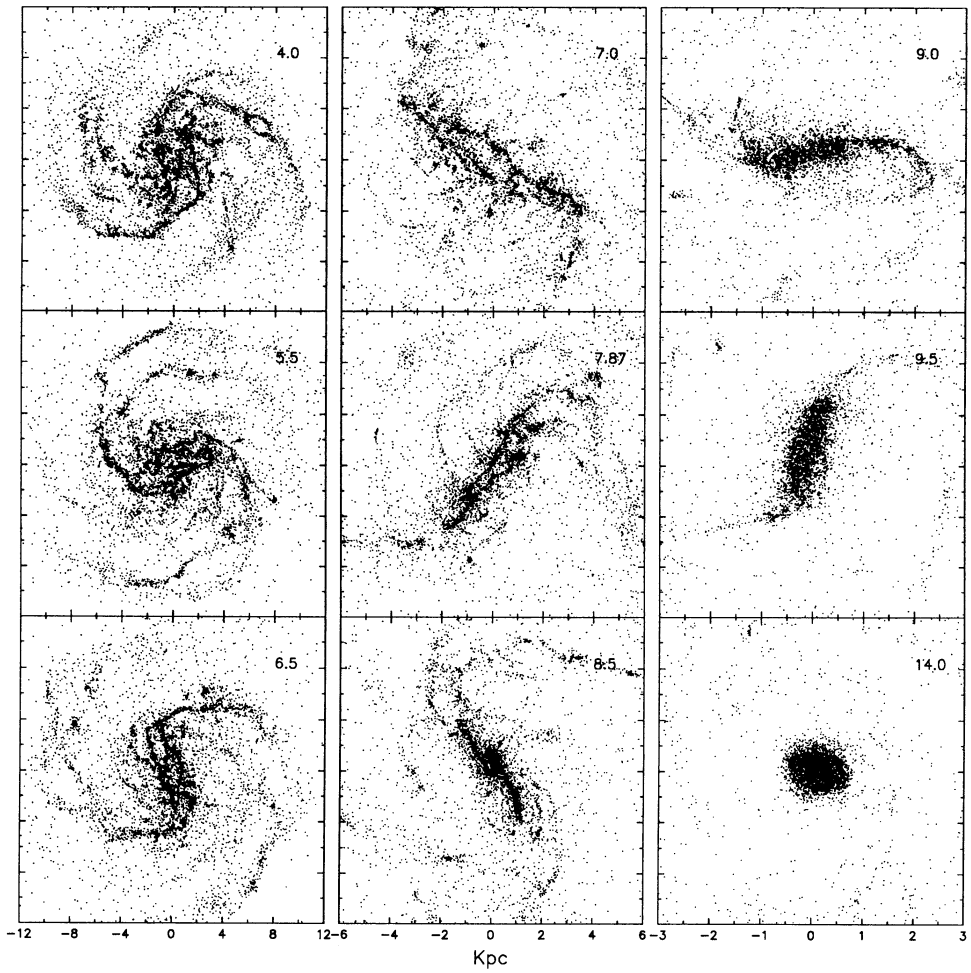

FIG. 11.—Evolution of gas in the globally unstable galactic disk model B10N with 10% gas, star formation ($\xi = 0.05$), and no "seed" BH, seen face-on. The time in units of τ_{dyn} is given in upper right corners. The frames are 24 kpc, 12 kpc, and 6 kpc in the left, middle, and right columns.

Similar damping of the bar instability because of the gravitational softening is well-known for pure stellar bars (Sellwood 1981). Independent of the ϵ_{min} used, the pattern speed of the gaseous bar is much larger than that of the large-scale stellar bar.

4.5. *Discussion*

The evolution of the gas distribution in disk galaxies appears to critically depend on its ability to form and sustain inhomogeneities. These inhomogeneities act as scattering centers and redistribute angular momentum. If the gas fraction exceeds a few percent of the total galactic mass, it affects the dynamics of the stellar component in the disk. For example, the gas can suppress a globally unstable stellar mode. In the absence of an energy source, such as OB stars and supernovae, which heats the ISM and limits the lifetime of massive clouds, the effect of clumpiness tends to be overestimated. Alternatively, ignoring the natural tendency of the ISM to clump results in unrealistic models. This underlines the basic philosophy of this study: to calculate a grid of models which cover the anticipated parameter space.

Our numerical simulations suggest that unless fragmentation is suppressed, by star formation or some other mechanism, the innermost gas in the disk evolves toward a massive binary cloud system (in the absence of a preexisting supermassive BH) through a hierarchy of successive mergers between clouds. During this process, some of the intercloud gas and stars are expelled from the central region while the binary merges and forms a single massive object at the center. This object accounts for $\sim$0.3–0.5 of the gas in the disk. Galaxies that show a double structure in the nuclear regions are known. For example, NGC 1614 in the mid-infrared displays a double starburst at the center, separated by 310 pc (Keto et al. 1991).

Unless the central BH is massive enough when it forms, say $>10^8\ M_\odot$, it will be either expelled from the center due to gravitational interactions with massive clouds (slingshot) or perform a random walk within the central 1 kpc. We observe that the feeding of a massive BH is dominated by the capture of clouds whose spin is misaligned with that of the galactic disk by as much as $\sim 20°$, while the orientation of the orbital angular momentum shows a much larger scatter. This may result in the rotation axis of the BH being misaligned with the rotation axis of the disk. However, such effects are beyond the scope of this paper. "Nailing down" the BH at the disk center enhances the $m = 2$ mode within the inner few hundred parsecs and damps the $m = 1$ model. The second effect may have interesting consequences for the angular momentum transfer in this region.

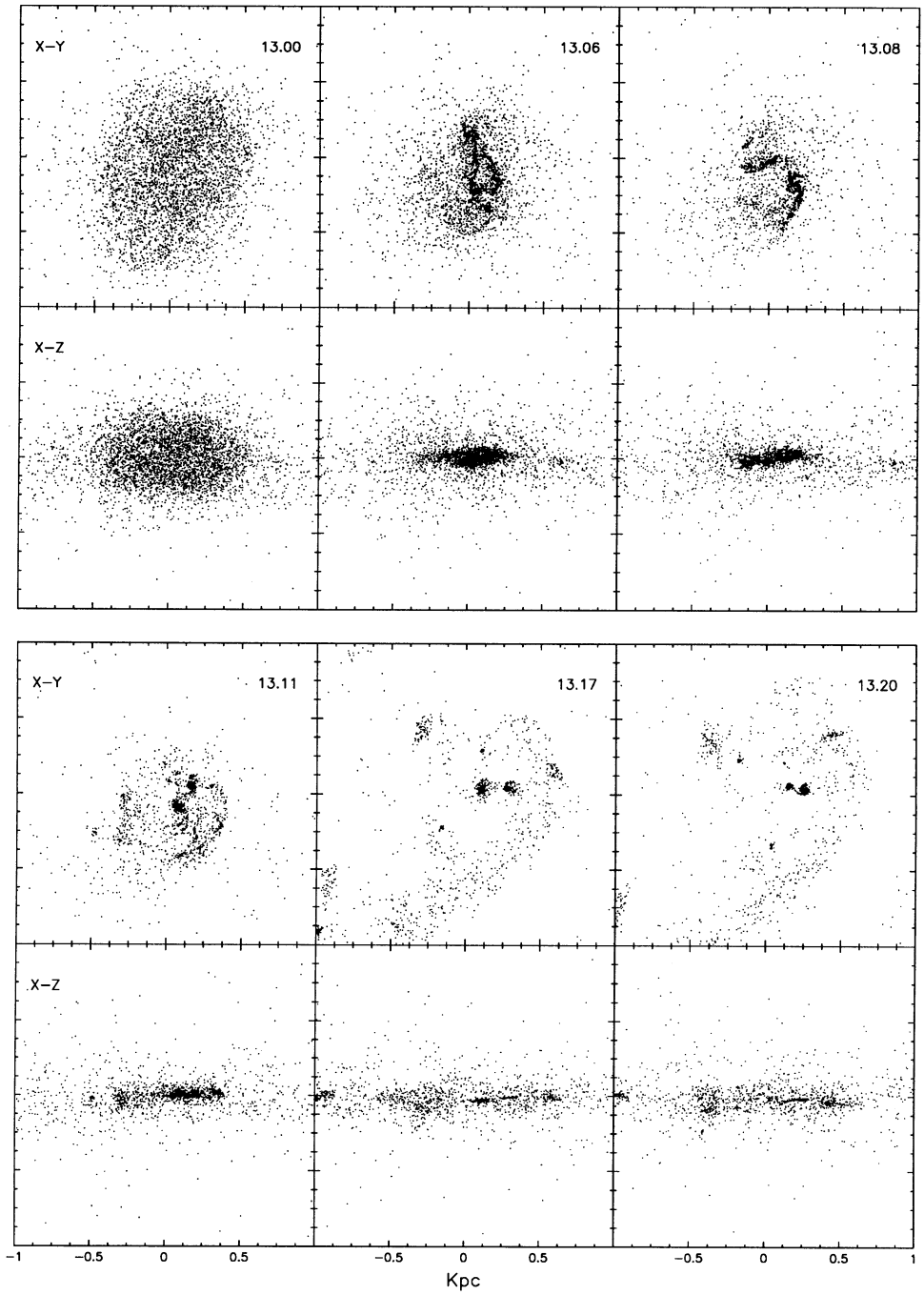

FIG. 12*a*

FIG. 12.—(*a*) Evolution of nuclear gaseous disk in the model B10Na (without the "seed" BH) after star formation was switched off, seen face-on and edge-on. The minimal softening length in the gas is $\epsilon_{min} = 7.5$ pc. All frames are 2 kpc. Initial mass of the nuclear disk is $\sim 4.7 \times 10^9 M_\odot$ within 1 kpc radius and $\sim 4.2 \times 10^9 M_\odot$ within 0.5 kpc radius. The mass of the binary cloud system at $\tau = 13.2\tau_{dyn}$ is $\sim 2.8 \times 10^9 M_\odot$. (*b*) Evolution of nuclear gaseous disk in the model B10Nb (without the "seed" BH) after star formation was switched off, seen face-on and edge-on. The minimal softening length in the gas is $\epsilon_{min} = 75$ pc. All frames are 2 kpc.

As the next logical step toward more realistic models, we have introduced star formation and a subsequent energy deposition by OB stellar winds and supernovae. A critical density of $\sim 100\ M_\odot\ \mathrm{pc}^{-3}$ in a locally gravitationally unstable gas was used as a threshold to activate the OB stars. Such a critical density is two orders of magnitude above the average gas density within 5 kpc in our models and almost four orders of magnitude above the gas density in the solar neighborhood. This choice has provided a negative feedback on the growth of Jeans instabilities in the gas on scales $\lesssim 100$ pc and limited the lifetime of Jeans unstable gas. The star formation process is, therefore, self-regulating, and only the rate of energy deposition by an OB star needs to be prescribed.

On larger scales, star formation affects the gasdynamics in the highly eccentric ring, preventing its fragmentation. At the same time, star formation induces shocks in the flow and the

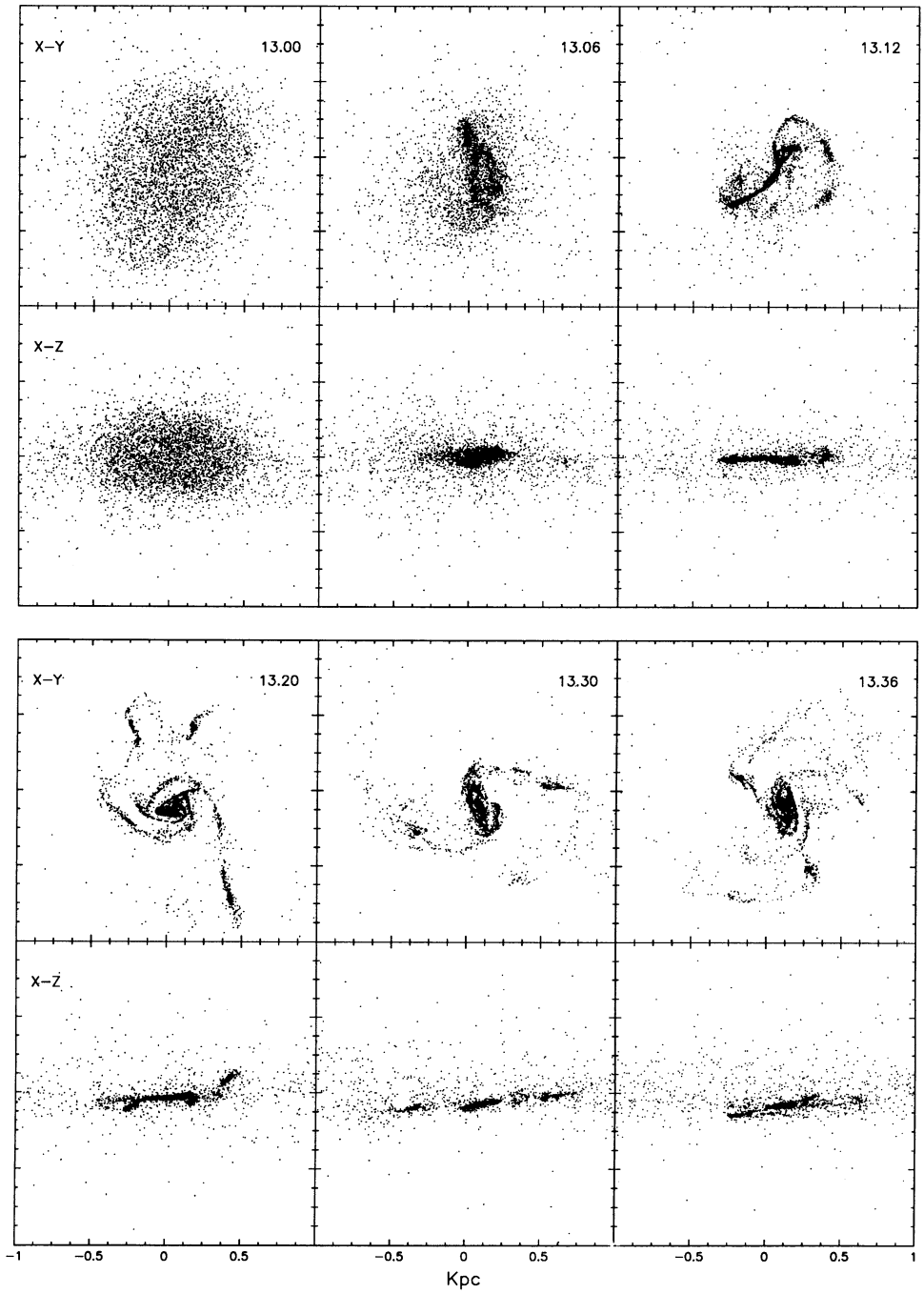

FIG. 12*b*

mixing of ring material with the surrounding gas, thus speeding up the angular momentum loss by the ring. As a result, the inflow grows faster and extends to smaller scales. The streaming along the gaseous ring is also dissipated by the K-H instability creating vortices along the ring's major axis. We did not attempt to calculate the actual contribution of this instability to the angular momentum loss by the gas, but, from indirect estimates, it does not exceed 10% of the contribution by the gravitational torques in our models. The general tendency of SPH to overestimate the shear viscosity may further shorten the vortice dissipation time. Given the general accuracy of our modeling, however, we do not expect this to affect the evolution of the gas distribution in the bar. Additional confirmation that our SPH code does not suffer from excessive shear viscosity comes from the fact that other methods for calculating inflow rates during the bar instability yield similar results (Shlosman & Noguchi 1993; Athanassoula 1993).

Star formation is concentrated initially at the apocenters of the gaseous circulation within the stellar bar and, at the climax of the inflow, in the nuclear region. In the gas-poor disks, i.e., those with fully developed stellar bars, only 10% of the gas remains at a distance $\sim$1–6 kpc, the rest is efficiently chan-

neled toward the center and becomes kinematically decoupled. In the gas-rich disks between $\sim$0.2–0.3 of the gas remains unaffected by dynamical friction. The central (<2 kpc) starburst phase is very luminous $\sim 10^{45}$–10^{46} ergs s^{-1} and exhibits an episodic character. A typical duration of a burst is $\sim 10^7$ yr and in excellent agreement with observations. Within the inner kiloparsec the gas reaches $\sim$20%–30% of the total mass in this volume. At the same time the gas is not in dynamical equilibrium, and $m = 1$–4 modes have significant amplitudes in the region. This coincides with catastropic accretion onto the "seed" BH which digests most of the gas. The remnant gas cools down and settles in a geometrically thin nuclear disk with a radius of $\sim$0.5–1 kpc and with a rotation axis misaligned by $\lesssim 10°$ from the galactic axis. Nuclear disks may have already been observed on several occasions (e.g., Ishizuki et al. 1990), and they do show some inclination to the galactic plane (NGC 4631, 5° inclination angle; see Sofue et al. 1991). Evolution of nuclear disks in the presence of star formation has been studied by Shlosman & Begelman (1989), who concluded that conventional viscosities are inefficient in fueling the BH under the conditions prevailing in these objects.

In the absence of the "seed" BH, the gas is not able to cool down quickly. Instead, it forms a fat disk supported both by the gas pressure (OB stars and supernovae energy deposition) and by rotation. We have demonstrated that these disks become globally unstable if and when the star formation declines. Gas inflows driven by this instability have similar rates as long as the minimal softening length is much smaller than the size of the system. When $\epsilon_{\rm min} > 100$ pc, it is expected to stabilize the global mode completely. Morphological differences between systems with different $\epsilon_{\rm min}$ become obvious from the onset of fission in the bar. The barlike mode dominates these disks and drives a self-similar inflow toward even smaller scales. Models with higher resolution exhibit fission of the gaseous bar which is followed by a coalescence of the major fragments. More theoretical work is required to understand the relationship of this inflow to the formation of the central BH itself. Observationally, the difficulties in detection of such dynamically unstable formations of molecular gas in the centers of galaxies are amplified by their short lifetime, which is less than 10^7 yr.

In all models (with and without BH and star formation) we see evolution of the mass concentration within the inner $\sim$100 pc up to $\sim 10^9\ M_\odot$ in less than two rotation periods, i.e., $\lesssim 6 \times 10^8$ yr. This trend seems to be independent from our choice of physical parameters, although a sharp increase in the kinetic-to-thermal energy conversion efficiency ξ in the nuclear region may limit the growth of the BH. We find that the increase of ξ by a factor of 4 results in a decrease in the BH mass by a factor of $\sim$1.5. In the dense environment of the central kiloparsec the efficiency of mechanical heating can sharply increase. This may happen if the supernovae rate becomes so high that shock heating of the ISM raises the gas temperature to $\sim 10^8$ K where the cooling rate is low and the high pressure can be sustained for a period of time longer than a sound-crossing time of the burst region. A supernova-driven wind is then possible (Chevalier & Clegg 1985; Heckman, Armus, & Miley 1990). This effect is neglected in our simulations. If much of the gas mass becomes locked up in low-mass stars, e.g., as in the Salpeter's IMF, the inflow along the large-scale stellar bar will be smaller. But it is not clear whether this will have a similar limiting effect on the growth of the BH.

Due to the fact that we model a galaxy which typically consists of $\sim 10^{11}$ stars using only $\sim$26,000 collisionless particles, it is relevant to ask to what extent this speeds up the two-body relaxation. An amplified rate of energy exchange between pairs of particles should artificially affect their orbits, introduce mass segregation (equipartition), and act as a source of numerical viscosity in a rotating stellar disk. All these effects limit the accuracy of the numerical simulations and must be taken into consideration when analyzing the evolution of the system. When $N \sim 10^4$ particles are used in the halo, the two-body relaxation timescale is $\tau_{2-b} \sim (0.1N/\ln N)\tau_{\rm dyn} \sim 100\tau_{\rm dyn}$ for Newtonian forces and $\sim 0.1N\tau_{\rm dyn}/\ln(R/\epsilon_*) \sim 250\tau_{\rm dyn}$ when gravitational softening $\epsilon_* = 200$ pc is implemented. We therefore expect the halo to be affected at the level of $\lesssim$10% during the simulation time. We note that spatial resolution for the stellar component is $\sim\epsilon_*$, and any features on smaller scale are purely numerical artifacts. This is not the case for the gaseous component, which has the dynamic gravitational softening and is able to resolve details on scales greater than the smoothing kernel $\epsilon_g \sim h$ (see § 3).

The effects of (numerical) two-body relaxation in disks have been studied by a number of authors (e.g., White 1985; White 1988; see Sellwood 1987 for a comprehensive review and references therein), who focus mainly on two-dimensional systems. Such relaxation is known to be very short, $\lesssim\tau_{\rm dyn}$, for razor-thin systems because the energy exchange is dominated by close encounters, unless the gravitational interaction is softened. In a three-dimensional system, the distant encounters contribute at least as much as the close encounters.

In our simulations, both the radial and the vertical structures of the stellar disk are resolved because the ratio of the softening to the disk radius is 0.02 and the ratio of the softening to the disk (Gaussian) width is $\sim$0.16 initially. Using the most stringent condition found in the literature to estimate the collisional effects in two-dimensional disks (Rybicki 1971), $\tau_{2-b} \sim \sigma_r^3\epsilon_*/\pi G^2\Sigma_* m_* \sim 2\pi Q_* N(\epsilon_*/R)(\sigma_r/v_\phi)^2\tau_{\rm dyn} \sim 50\tau_{\rm dyn}$, where m_* is the mass of a single particle and Σ_* is the surface density in the stellar disk. The use of the softening parameter in the above formula can be interpreted as introducing an effective thickness of the disk $\sim\epsilon_*$. Keeping in mind that our disk is resolved vertically, this estimate should provide a strong upper limit for the strength of relaxation effects due to the gravitational encounters. The importance of the two-body relaxation in the disk can also be measured by observing changes in the global characteristics of the system, such as the density and the rotation velocity profiles, as well as local parameters, such as dispersion velocities whose evolution reflects the degree of numerical "noise" in the model. We therefore ran a test model of a global *stable* stellar disk embedded in the live halo with the halo-to-disk mass ratio of 4:1. All other parameters have been kept unchanged compared to our A0 model, including the Toomre parameter $Q_* = 1.5$, which serves as a measure of radial dispersion velocities σ_r. We find that at the end of the simulations (after five rotations) the density and rotational velocity distributions changed by less than 10%, except at the outer edge where some particles have diffused outward to smooth the initially sharp cutoff. The Q_* has increased to 1.97 at $r = 3$ kpc (31% change) and to 1.83 at $r = 8$ kpc (22%). This increase is almost entirely due to the growth of the radial dispersion velocities in the initially cold disk ($Q_* = 1.5$) and is consistent with the heating by transient spiral instabilities appearing in the disk, as was shown by Sellwood & Carlberg (1984) in the two-dimensional numerical simulations with 20,000 particles. During the same interval of time, the vertical velocity dispersion increased by a smaller amount, $\sim$16% and $\sim$11%, at 3 kpc and 8 kpc respectively.

The thickness of the globally *unstable* stellar disk (model A0) within the inner ~ 4 kpc is affected by the so-called bending (or fire hose) instability (A. Toomre, 1988 private communication) of the bar, which has been recently addressed in numerical simulation by Raha et al. (1991) and which shows up in our simulations between $\tau \sim 15$–$19\tau_{dyn}$. This instability results from *collective* effects, weakens the bar, and is responsible for the peanut-shape morphology of the inner disk thereafter. The fact that our stellar disks display a violent bar instability and that the formed bar is subject to bending instability further confirms our estimates that the excessive disk heating by the two-body interactions does not govern the evolution during the simulations. To verify this, we have repeated the unstable A0 model with 32,768 particles in the disk. Again, after five rotations, the rotation curve and the density profiles, as well as the bar characteristics, differ by less than 10% between the models. If two-body relaxation would dominate the dynamics, the differences by a factor of 2 are expected. On the other hand, as it was shown by Sellwood (1983), the pattern speed in disk models does not depend in a sensitive way on the number of particles used in the simulations and lies close to the value predicted by the linear theory. We conclude, therefore, that the two-body relaxation has a negligible effect on the evolution of our system. The accuracy of these simulations is sufficient to catch the major dynamical processes in the stellar component which are used to study the gasdynamics in the stellar disks. It is also clear that in order to follow the *secular* evolution of this system, a much larger number of particles, $\gtrsim 10^5$, should be used.

An additional comment is related to the interaction between the halo and large-scale stellar bar. As a result of the gravitational torque by the bar, the halo acquires some rotation and flattens, especially in the inner few kiloparsecs. Based on our simulations, we expect the secular evolution of the stellar bar's pattern speed on a Hubble timescale in pure stellar disks. This is slower but in basic agreement with the recent results by Hernquist & Weinberg (1992). The inefficient angular momentum transfer from the bar to the halo is due to the supression of resonance interactions between these components. The reason for this is a relatively small number of halo particles employed in our simulations. However, the two-body interaction between the bar and the halo is still neglibible during the simulation time of about five bar revolutions ($\Omega_b/\Omega_{eq} \sim 50$, where Ω_{eq} is the equipartition angular velocity of the bar estimated by Weinberg 1985). As we focus on the gas response to the global dynamical instability and limit the evolution to a few bar rotations only, our bar should not be slowed down by this numerical relaxation. In fact, continuous gas inflow toward the center, which we observe on a much shorter timescale, leads to an opposite effect owing to the increased precession rate of stellar orbits in the bar. The net trend seems to be that the bar's pattern speed stays constant or slightly increases for as long as the inflow occurs.

5. CONCLUSIONS

In order to study the fate of dynamically important gas configurations in the central regions of disk galaxies, we have constructed a globally unstable model of a two-component disk embedded in a responsive halo. The gravitational interactions between the gas, stars, and halo particles are fully accounted for. The radial gas inflow was triggered by a large-scale stellar bar or by dynamical friction, depending on the gas fraction. For models without star formation, the overall evolution of gas toward the inner kiloparsc is similar to that discussed in Shlosman & Noguchi (1993). The new result here is the development of a highly eccentric gaseous ring, reflecting the transition between simple and more complex x_1 orbits possessing end loops. The initial semimajor axis of the ring is of the order to the stellar bar radius (and of the velocity turnover radius), and its semiminor axis is comparable to that of the bar. The ring grows in mass, fragments, and becomes increasingly eccentric. For the gas-poor disks the ring appears to be robust, and the fragments stay within it. The hydrodynamical and gravitational interactions in the ring distort it and bring about the gravitational torque from the stellar bar depriving gas of much of its angular momentum. The inflow peak rates are in the range of 1–25 $M_\odot$ yr^{-1} for the gas fraction of $\simeq 0.01$–0.15, although these numbers must be taken as upper limits because we neglect the gas lockup in low-mass stars.

Our main results concern the dynamical state of gas within the inner 1 kpc, where for models *without* star formation we find that 1) a few massive clouds dominate the dynamics and evolve toward a single massive object in the center, with and without a "seed" BH, for a wide range of parameters; 2) accretion and growth of the central BH has a sporadic character; and 3) as a result of the capture and digestion of clouds by the BH remnant disks form with the radius of 60–80 pc.

Models *with* star formation suppress the fragmentation in the elliptical ring and elsewhere in the disk. We find that in the presence of a seed BH, these models are characterized by 1) increased mixing in the gas confined to the stellar bar, inducing angular momentum loss and inflow rate by a factor of <3; 2) star formation which is concentrated at the apocenters of the gaseous circulation in the stellar bar and in the nuclear region; 3) a central starburst phase which is very luminous, $\sim 10^{45}$–10^{46} ergs s^{-1}, and episodic, with a typical burst duration of $\sim 10^7$ yr; 4) a correlation between the nuclear starburst, the peak accretion rate onto the central BH, and the gas-to-dynamical mass ratio within 1 kpc reaching ~ 0.2–0.3; and by 5) formation of cold nuclear disks within a few hundred parsecs, inclined to the galactic plane by $\lesssim 10°$.

Nuclear disks also form in models with star formation and *without* the seed BH. The starburst phase is prolonged in this case, and the disks remain hot and geometrically thick. If star formation declines, they rapidly cool down and become bar unstable. These disks contain $\sim 50\%$ of the total dynamical mass within 500 pc. The subsequent evolution 1) drives a self-similar inflow toward even smaller scales, when the Jeans instability in the gas is suppressed, or 2) leads to fission in the gaseous bar and formation of a massive cloud binary system at the center.

This work outlines the complicated physical conditions in the central regions of disk galaxies. Our modeling has exposed alternatives in the dynamical evolution of self-gravitating gas which may ultimately lead to a luminous starburst and the formation of a supermassive object at the center of an active galaxy. We show numerically that these phenomena may be causally related and constitute a normal evolutionary phase for disk galaxies. The importance of gravitational instabilities in the stellar disk and in the central gas accumulation has been demonstrated, and our major conclusions support the "bars in bars" model of Shlosman et al. (1990).

We caution against overinterpreting our results. Some numbers quoted in this work, such as the inflow rates, should serve as reference numbers to within an order of magnitude only. Others, such as the gas mass fraction, which can suppress

the stellar bar instability, are uncertain to within a factor of 2. Although the evolutionary pattern displayed by the numerical models seems to be robust, the physics of star formation as well as the multiphase character of the ISM could modify it. We have omitted a self-consistent calculation of radiative cooling in the ISM. Radiative processes become especially important within the central 1 kpc, where the massive star-formation rate is largest. A simple approximation for cooling will be incorporated in our numerical scheme, which will enable us to address the formation of supernovae-driven winds from the nuclei of starburst galaxies. Another subject, which deserves much more attention and which is currently being investigated, is the evolution of gaseous bars in the inner few hundred parsecs. And finally, a high-resolution study of gas flows in stable stellar bars is in progress (Shlosman & Heller 1993) in order to achieve a more complete picture of fueling mechanisms of central activity in disk galaxies.

We are grateful to Juhan Frank and Masafumi Noguchi for numerous discussions and constructive criticism, to Dimitris Christodoulou for his comments on the stability of self-gravitating nuclear disks, and to Chris Kochanek for discussing the SPH. We thank the Center of Computational Sciences and its Director John Connolly for continuous support. Calculations were performed on IBM 3090-600J at the University of Kentucky Supercomputing Center.

REFERENCES

Adams, T. F. 1977, ApJS, 33, 19
Athanassoula, E. 1984, Phys. Rep., 114, 319
———. 1992a, MNRAS, 259, 328
———. 1992b, MNRAS, 259, 345
———. 1993, in Proc. Intern. Conf. on Mass-Transfer Induced Activity in Galaxies, ed. I. Shlosman (Cambridge: Cambridge Univ. Press), in press
Athanassoula, E., Bienayme, O., Martinet, L., & Pfenniger, D. 1983, A&A, 127, 349
Balbus, S. A. 1988, ApJ, 324, 60
Balzano, V. A. 1983, ApJ, 268, 602
Barnes, J., & Hut, P. 1986, Nature, 324, 446
Begelman, M. C., Blandford, R. D., & Rees, M. J. 1980, Nature, 287, 307
———. 1984, Rev. Mod. Phys., 56, 255
Bertin, G., Lin, C. C., Lowe, S. A., & Thurstans, R. P. 1989, ApJ, 338, 78
Binney, J., & Tremaine, S. 1987, Galactic Dynamics (Princeton: Princeton Univ. Press)
Braine, J., & Combes, F. 1992, A&A, 264, 433
Chandrasekhar, S. 1969, Ellipsoidal Figures of Equilibrium (New Haven: Yale Univ. Press)
Chevalier, R. A. 1974, ARA&A, 15, 175
Chevalier, R. A., & Clegg, A. W. 1985, Nature, 317, 44
Christodoulou, D. M., & Narayan, R. 1992, ApJ, 388, 451
Combes, F., & Gerin, M. 1985, A&A, 150, 327
Condon, J. J. 1983, ApJS, 53, 459
Contopoulos, G., & Papayannopoulos, T. 1980, A&A, 92, 33
Cox, J. P. 1980, Theory of Stellar Pulsation (Princeton: Princeton Univ. Press)
de Vaucouleurs, G., de Vaucouleurs, A., & Corwin, H. 1976, Second Reference Catalogue of Bright Galaxies (Austin: Univ. of Texas)
Devereux, N. A. 1987, ApJ, 323, 91
Dressel, L. L. 1988, ApJ, 329, L69
Emmering, R. T., Blandford, R. D., & Shlosman, I. 1992, ApJ, 385, 460
Fall, S. M., & Efstathiou, G. 1980, MNRAS, 193, 189
Friedli, D., & Benz, W. 1993, A&A, 268, 65
Fukunaga, M., & Tosa, M. 1991, PASJ, 43, 469
Garcia-Barreto, J. A., Downes, D., Combes, F., Gerin, M., Magri, C., Carrasco, L., & Cruz-Gonzales, I. 1991, A&A, 244, 257
Goodman, J., & Narayan, R. 1988, MNRAS, 231, 97
Hackwell, J. A., & Schweizer, F. 1983, ApJ, 265, 643
Hawarden, T. G., Mountain, C. M., Leggett, S. K., & Puxley, P. J. 1986, MNRAS, 221, 41P
Heckman, T. M., Armus, L., & Miley, G. K. 1990, ApJS, 74, 833
Heller, C. H. 1991, Ph.D. thesis, Yale Univ.
Henkel, C., Baan, W. A., & Mauersberger, R. 1991, A&A Rev., 3, 47
Hernquist, L. 1987, ApJS, 64, 715
———. 1989, Nature, 340, 687
Hernquist, L., & Katz, N. 1989, ApJS, 70, 419
Hernquist, L., & Weinberg, M. D. 1992, ApJ, 400, 80
Hummel, E. 1981, A&A, 93, 93
Hunter, C. 1963, MNRAS, 126, 299
Huntley, J. M. 1978, ApJ, 225, L101
Huntley, J. M., Sanders, R. H., & Roberts, W. W. 1978, ApJ, 221, 521
Ishizuki, S., et al. 1990, ApJ, 355, 436
Jackson, J. M., Barrett, A. H., Armstrong, J. T., & Ho, P. T. P. 1987, AJ, 93, 531
Julian, W. H., & Toomre, A. 1966, ApJ, 146, 810
Kenney, J. D. P., Wilson, C. D., Scoville, N. Z., Devereux, N., & Young, J. S. 1992, ApJ, 395, L79
Kennicutt, R. C. 1989, ApJ, 344, 171
Kennicutt, R. C., Keel, W. C., van der Hulst, J. M., Hummel, E., & Roettiger, K. A. 1987, AJ, 93, 1011
Keto, E., Ball, R., Arens, J. F., Jernigan, G., & Meixner, M. 1991, in Proc. IAU Symp. 146, Dynamics of Galaxies and Their Molecular Cloud Distributions, ed. F. Combes & F. Casoli (Dordrecht: Kluwer), 433
Koribalski, B., Dickey, J. M., & Mebold, U. 1993, ApJ, 402, L41
Kormendy, J. 1982, in Morphology and Dynamics of Galaxies, ed. L. Martinet & M. Mayor (Geneva: Geneva Observatory), 115
Lipari, S., Tsvetanov, Z., & Macchetto, F. 1993, ApJ, 405, 186
Lubow, S. H. 1988, ApJ, 328, L3
Lubow, S. H., Balbus, A., & Cowie, L. L. 1986, ApJ, 309, 496
Lucy, L. 1977, AJ, 82, 1013
Meixner, M., Puchalsky, R., Blitz, L., Wright, M., & Heckman, T. 1990, ApJ, 354, 158
Monaghan, J. J. 1982, SIAM. J. Sci. Statist. Comput., 3, 422
———. 1988, Comput. Phys. Comm., 48, 89
———. 1992, ARA&A, 30, 543
Monaghan, J. J., & Gingold, R. A. 1983, J. Comput. Phys., 52, 374
Noguchi, M. 1988, A&A, 201, 37
Norman, C. A. 1988, in Star Formation in Galaxies NASA CP-2466, 395
Pfenniger, D., & Friedli, D. 1991, A&A, 252, 75
Puxley, P. J., Hawarden, T. G., & Mountain, C. M. 1988, MNRAS, 231, 465
Raha, N., Sellwood, J. A., James, R. A., & Kahn, F. D. 1991, Nature, 352, 411
Rieke, G. H., Lebofsky, M. J., Thompson, R. I., Low, F. J., & Tokunaga, A. T. 1980, ApJ, 238, 24
Rieke, G. H., Loken, K., Rieke, M. J., & Tamblyn, P. 1993, ApJ, submitted
Rybicki, G. B. 1971, in IAU Colloq. 10, Gravitational *N*-Body Problem, ed. M. Lecar (Dordrecht: Reidel), 22
Salpeter, E. E. 1976, ApJ, 206, 673
Sandage, A., & Tammann, G. A. 1981, A Revised Shapley-Ames Catalog of Bright Galaxies, Carnegie Inst. Washington Publ., No. 635
Sanders, R. H., & Tubbs, A. D. 1980, ApJ, 235, 803
Scalo, J. M. 1989, in Windows on Galaxies, ed. A. Renzini et al. (Dordrecht: Kluwer), p. 000
Scalo, J. M., & Struck-Marcell, C. 1986, ApJ, 301, 77
Sandage, A., & Tammann, G. A. 1981, A Revised Shapley-Ames Catalog of Bright Galaxies, Carnegie Inst. Washington Publ., No. 635
Sanders, R. H., & Tubbs, A. D. 1980, ApJ, 235, 803
Scalo, J. M. 1989, in Windows on Galaxies, ed. A. Renzini et al. (Dordrecht: Kluwer)
Scalo, J. M., & Struck-Marcell, C. 1986, ApJ, 301, 77
Schwarz, M. P. 1984, MNRAS, 209, 93
Scoville, N., Matthews, K., Carico, D. P., & Sanders, D. B. 1988, ApJ, 327, L61
Schoville, N., Thakkar, D., Carlstrom, J. E., & Sargent, A. I. 1993, preprint
Scoville, N. Z., Hibbard, J. E., van Gorkom, J. H., & Yun, M. S. 1993, in Proc. Intern. Conf. on Mass-Transfer Induced Activity in Galaxies, ed. I. Shlosman (Cambridge: Cambridge Univ. Press), in press
Sellwood, J. A. 1981, A&A, 99, 362,
———. 1983, J. Comput. Phys., 50, 337
———. 1987, ARA&A, 25, 151
———. 1992, in Proc. Symp. Interstellar Matter in Galaxies (Prague)
Sellwood, J. A., & Carlberg, R. G. 1984, ApJ, 282, 61
Sellwood, J. A., & Wilkinson, A. 1993, Rep. Prog. Phys., 56, 173
Shlosman, I., & Begelman, M. C. 1989, ApJ, 341, 685
Shlosman, I., Begelman, M. C., & Frank, J. 1990, Nature, 345, 679
Shlosman, I., Frank, J., & Begelman, M. C. 1988, in Proc. IAU Coll. 134, Active Galactic Nuclei, ed. D. Osterbrock & J. Miller (Dordrecht: Kluwer), 462
Shlosman, I., Frank, J., & Begelman, M. C. 1989, Nature, 338, 45
Shlosman, I., & Heller, C. H., in preparation
Shlosman, I., & Noguchi, M. 1993, ApJ, 414, 474
Simkin, S. M., Su, H. J., & Schwarz, M. P. 1980, ApJ, 237, 404
Sofue, Y. 1991, in Proc. IAU Symp. 146, Dynamics of Galaxies and Their Molecular Gas Distributions, ed. F. Combes & F. Casoli (Dordrecht: Kluwer), 287
Sofue, Y., Handa, T., Golla, G., & Wielebinski, R. 1991, PASJ, 42, 745
Sorensen, S. A., Matsuda, T., & Fujimoto, M. 1976, Ap&SS, 43, 491
Sparke L. S., & Sellwood, J. A. 1987, MNRAS, 225, 653
Spitzer, L. 1978, Physical Processes in the Interstellar Medium (New York: Wiley)
Telesco, C. M. 1988, ARA&A, 26, 343
Thronson, H. A., et al. 1989, ApJ, 343, 158
Toomre, A. 1962, ApJ, 138, 385

Toomre, A. 1964, ApJ, 139, 1217
———. 1981, in Structure & Evolution of Normal Galaxies, ed. M. Fall & D. Lynden-Bell (Cambridge: Cambridge Univ. Press), 111
Turner, J. 1993, in Proc. Intern. Conf. on Mass-Transfer Induced Activity in Galaxies, ed. I. Shlosman (Cambridge: Cambridge Univ. Press), in press
van Albada, G. H., & Roberts, W. W. 1981, ApJ, 246, 740
Wada, K., & Habe, A. 1992, MNRAS, 258, 82
Wakamatsu, K., & Nishida, M. T. 1980, PASJ, 32, 389
Weinberg, M. D. 1985, MNRAS, 213, 451
Whitehurst, R. 1988, MNRAS, 233, 529
White, R. L. 1988, ApJ, 330, 26
White, S. D. M. 1983, ApJ, 274, 53
Wright, G. S., Joseph, R. D., Robertson, N. A., James, P. A., & Meikle, W. P. S. 1988, MNRAS, 233, 1
Wrobel, J. M., & Kenney, J. D. P. 1992, ApJ, 399, 94
Young, J. S., & Scoville, N. Z. 1991, ARA&A, 29, 581